Evaluation of active components and pharmacological activities by UPLC-Q/TOF-MS and network pharmacology in *Lentinula edodes* and *Lyophyllum decastes*

Yingnan Zhang, Gaoxing Ma, Fei Pei, Ning Ma, Anxiang Su, Qiuhui Hu, Meng Wang*

College of Food Science and Engineering, Nanjing University of Finance and Economics/Collaborative Innovation Center for Modern Grain Circulation and Safety, Nanjing, China

***Corresponding Author:** Meng Wang, College of Food Science and Engineering, Nanjing University of Finance and Economics/Collaborative Innovation Center for Modern Grain Circulation and Safety, Nanjing 210023, China. Email: mwang@nufe.edu.cn

Academic Editor: Teresa D'Amore, PhD, Chemistry Department, Experimental Zooprophylactic Institute of Puglia and Basilicata, Via Manfredonia 20, 71121 Foggia, Italy

Received: 28 March 2024; Accepted: 14 October 2024; Published: 21 December 2024

ORIGINAL ARTICLE

Abstract

Lentinula edodes (*L. edodes*) is a premium edible fungus cultivated extensively throughout China, and *Lyophyllum decastes* (*L. decastes*) is a wild edible fungus with a high degree of industrial-level cultivation in China. Regarding the edible value of the two fungi, research on their medicinal properties is relatively scarce. In this study, we utilized ultra-high performance liquid chromatography with quadrupole and time-of-flight mass spectrometry to analyze comprehensively the chemical composition of both fungi. In all, 120 and 144 chemical components were identified in *L. edodes* and *L. decastes*, respectively. Subsequently, we elaborated active components, potential biological activities, and therapeutic targets associated with both fungi by using network pharmacology. The results showed that seven active components in *L. edodes* and nine active components in *L. decastes* could act on common targets, such as AKT serine/threonine kinase1 and peroxisome proliferator-activated receptor gamma, thereby regulating signaling pathways, such as epidermal growth factor receptor and mitogen-activated protein kinase, to affect the body. In addition, these components affect immune regulation and inhibition of liver cancer. Finally, we used cell experiments to verify their activities. Our findings provided a reliable foundation for future research aimed at harnessing the bioactivities of *L. edodes* and *L. decastes*, thereby offering novel strategies for their utilization in the field of functional foods and natural medicine.

Keywords: edible fungi; active components; pharmacological activities; UPLC-Q/TOF-MS; network pharmacology

Introduction

Lentinula edodes (*L. edodes*) is a widely consumed fungus classified under the taxonomic hierarchy of *fungi, Basidiomycota, Agaricomycetes, Agaricales, Omphalotaceae,* and *Lentinula.* Its natural distribution includes warm and moist climates of Southeast Asia (Roszczyk *et al.*, 2022). Presently, it is found all over the world because of its artificial planting. *L. edodes* is rich in polysaccharides, dietary fiber, protein, and other nutrients, and has been used as an edible source of food for thousands of years in Asian and European countries. *L. edodes* is also considered a medicinal fungus in traditional Chinese medicine (TCM); its pharmacological effects have long been mentioned in TCM classics.

Lyophyllum decastes (*L. decastes*) is a wild edible and medicinal fungus classified within the taxonomic

hierarchy of *fungi*, *Basidiomycota*, *Agaricomycetes*, *Agaricales*, *Lyophyllaceae*, and *Lyophyllum*. China is the largest producer of *L. decastes* globally, and its 2020 yield in China was about 11,590 tons (Xu *et al.*, 2023). *L. decastes* has delicate flesh, fragrant aroma, delicious taste, and is rich in proteins, minerals, and polysaccharides. It is recorded in Chinese Materia Medica that *L. decastes* can stop bleeding, detoxify, and treat breast cancer and hemangiomas (Lin, 2012).

Several studies have reported the biological activities of the crude extracts or related products of both fungi *in vivo* as well as *in vitro*. Hye-Lim *et al.* (2017) estimated antioxidant activities of different extracts of *L. edodes*. Among them, water extract exhibited the strongest 2,2-Diphenyl-1-picrylhydrazyl (DPPH), 2,2'-azino-bis (3-ethylbenzothiazoline-6-sulfonic acid positive ($ABTS^+$) radicals, and nitrite scavenging activities. Hot water extracts of *L. decastes* can induce the production of interferon-gamma (IFN-γ) and interleukin-4 (IL-4) in mice and enhance T cells immune activity (Ike *et al.*, 2012). Nevertheless, these studies assessing the biological activities of fungi were not exhaustive, as they merely provided a brief evaluation of their primary component and its specific active functions (Dai *et al.*, 2023a).

Many studies demonstrated different effects of various bioactive components of edible fungi on the body, and these components are often multifunctional in biological activity (Li *et al.*, 2022). They have multiple targets through which they regulate biological processes and signaling pathways of the body (Garcia *et al.*, 2022). Phytochemical profile analysis is a key step in the development and utilization of plant resources and quality safety assurance. So far, research on the composition of the two fungi has mainly involved the nutritional composition (Gameli-Kwabla, 2020; Nayik *et al.*, 2023), polysaccharides (Dai *et al.*, 2023b; Zhang *et al.*, 2023), and volatile components (Fujita *et al.*, 2021; Wang *et al.*, 2021) of the fruiting body, mycelium and fermentation broth. Literature reports also described the small-molecule chemical composition of both fungi. A number of techniques have been developed to analyze the composition of fungi, such as headspace solid-phase microextraction, gas chromatography–mass spectrometry, electronic nose for volatile substances (Lu *et al.*, 2022), and high-performance liquid chromatography (HPLC), and nuclear magnetic resonance (NMR) for other substances (Ding *et al.*, 2022).

Immune system diseases (ISD), also known as immunological disorders, arise from dysfunctions within the immune system, which is responsible for maintaining homeostasis and safeguarding the health. These ISDs result in the immune system erroneously attacking its own tissues and molecules, leading to a variety of debilitating conditions (Wen *et al.*, 2024). Virtually, all pathological states in organ tissues are intricately linked to the immune system. Infections, autoimmunity, immune deficiencies, antigen responses, cancer development, and various other conditions are intricately connected to the functioning of the immune system. Alternatively, cancer disease (CD) is often referred to as the "king of all diseases" because of its ability to affect nearly every part and organ of the human body. Cancer is the first or second leading cause of premature deaths (at ages 30–69 years) globally (Xie *et al.*, 2021). According to the World Health Organization (WHO), cancer is one of the main causes of death in humans, with 10 million (nearly one in six) deaths in 2020 attributed to cancer. There exists an interactive and complex relationship between ISDs and cancer. In addition to predisposing individuals to ISDs, an imbalance in the immune system may also facilitate the evasion of cancer cells from detection and foster their growth within the body (Li *et al.*, 2021). In contrast, cancer cells possess diverse mechanisms to interfere the immune system, thus promoting immune evasion. Consequently, patients often exhibit signs of immunosuppression, rendering them more vulnerable to infections with other pathogens (Starzer *et al.*, 2022).

Many studies have shown diverse health effects of fungi because of the presence of a variety of bioactive components (Cui *et al.*, 2022; Yin *et al.*, 2022). Ultra-high performance liquid chromatography with quadrupole and time-of-flight mass spectrometry (UPLC-Q–TOF-MS), with the advantages of high speed, high resolution, and high precision, is a mass spectrometry technology used to integrate separation and detection analysis. The technology is extensively employed in investigating the chemical components and active constituents of natural medicines (Liang *et al.*, 2021). It also disintegrates the metabolic kinetics of pharmacodynamic components combined with network pharmacology (Qiu *et al.*, 2024). Network pharmacology is a combined technology of computer application and systems biology, used to explore the complex network of interactions between drugs and biological systems. This approach helps to understand the multi-target mechanisms of drugs, their adverse effects, and potential new uses (Zhu *et al.*, 2023). Du *et al.* (2024) confirmed that phosphoinositide 3-kinase–protein kinase B (PI3K/AKT) signaling pathway could probably be the mechanism by which pachymic acid could effectively treat gastric cancer by network pharmacology. Xu *et al.* (2024) used network pharmacology to confirm that the mechanism of Res against glycogenin (GN) could be the regulation of arachidonic acid metabolism by regulating prostaglandin-endoperoxide synthase 1 (*PTGS1*) and *PTGS2*.

For better utilization of *L. edodes* and *L. decastes* resources, it is crucial to conduct an exhaustive analysis

of their chemical constituents and biological properties. The primary objective of this study was to conduct a comprehensive assessment of the chemical composition and bioactivity of both fungi. Owing to the lack of systematic analysis of the components and complex pharmacological effects of both edible fungi, this study aimed to elucidate through cell experiments the principal active constituents present in two fungi, along with identifying their pharmacodynamic targets. Such insights are pivotal for validating their clinical applications and fostering the continued development of both fungal resources.

Materials and Methods

Analysis through UPLC-Q–TOF-MS

Chemicals and reagents

Chromatography-grade methanol, acetonitrile, and formic acid were purchased from Sigma-Aldrich (St. Louis, MO, USA). Deionized water (18.3 MΩ) was generated by a Milli-Q water purification system obtained from Millipore Ltd. (Bedford, MA, USA). Macrophages RAW264.7 were purchased from Pricella Biotechnology Co. (Wuhan, China). The liver cancer cells HepG-2 were purchased from Beyotime Biotechnology (Nanjing, China). Dulbecco's Modified Eagle Medium (DMEM), penicillin/streptomycin, and phosphate-buffered saline (PBS) solution were purchased from Thermo Fisher Scientific Inc. (Nanjing, China). CCK-8 kit and neutral red kit were purchased from Beyotime Biotechnology. *L. edodes* and *L. decastes* were collected from Yunnan Bacteria Horizon Biotechnology Co. (Yunnan, China).

Preparation of Samples

In all, 1.0 g of fungi freeze-dried material was weighed, placed in a 50-mL centrifuge tube, and extracted with 20 mL of methanol–water (1:1, v/v). The solution was vortexed for 1 min, ultrasonicated at room temperature for 30 min, centrifuged at 4°C with 12,000 r/min for 10 min at 4°C; 1 mL of the supernatant was filtered using a 0.22-μm nylon membrane.

Instrumentation

Sepax GP-C18 column (1.8 μm, 120 Å, 2.1 mm × 150 mm). Each component was gradient eluted for 21 min. The mobile phase was (a) 0.01% formic acid and (b) 100% acetonitrile. The flow rate was maintained at 0.3 mL/min, with column temperature of 40°C and an injection volume of 2 μL (Table 1). Electrospray ionization (ESI) with positive ion and negative ion modes was used for detection. ESI source conditions were as follows: ion spray voltage 5,500 V in positive ion mode, gas 50 psi, temperature 500°C; negative ion mode 4,400 V, gas 50 psi, temperature 450°C; curtain gas 25 psi; time-of-flight–mass spectrometry (TOF-MS) scanning range: 100–1,200 Da; ion scanning range: 50–1,000 Da; TOF/MS scan accumulation time 0.2 s; product ion scan accumulation time 0.01 s; secondary mass spectrometry using high sensitivity mode and information-dependent acquisition, declustering voltage ±60 V, and collision energy 35±15 eV.

Table 1. Gradient elution procedure conditions.

Elution time(min)	Phase A (%)	Phase B (%)
0	95	5
10	30	70
17	0	100
18	0	100
19	95	5
21	95	5

Database search and comparison of fungi components

The mass spectrometry acquisition .wiff file was preprocessed by the software MS-DIAL 4.70, including peak extraction, denoising, deconvolution, peak alignment, and export of a three-dimensional (3D) data matrix in comma-separated value (CSV) format. The extracted peak information was compared with the database GNPS (https://gnps.ucsd.edu/), Respect (http://spectra.psc.riken.jp/), and MassBank (https://massbank.eu/MassBank). The databases were searched in their entirety and matched according to the parameters shown in Table 2. This 3D matrix includes the following information: sample information, retention time, mass-to-nuclear ratio, and mass spectrometry response intensity.

Analysis of network pharmacology

Target prediction of L. edodes and L. decastes

First, the active components of *L. edodes* and *L. decastes* were screened by the SwissADME (http://www.swissadme.ch/) platform and literature. At SwissADME platform, gastrointestinal absorption (GA), one of the

Table 2. Database matching parameters.

Classification	Parameters	Setting
Peak detection parameters	Minimum peak height	1,000 amplitude
	Mass slice width	0.1 Da
Alignment parameters	Retention time tolerance	0.05 min
	MS1 tolerance	0.015 Da
Identification setting	Accurate mass tolerance (MS1)	0.01 Da
	Accurate mass tolerance (MS2)	0.05 Da
	Identification score cut off	80

pharmacokinetic parameters, was set at "HIGH" as a condition for drug absorption, and active compounds with good oral bioavailability were screened. Likewise, the drug-likeness (DL) was also considered for cosmeceutical parameters (Lipinski, Ghose, Veber, Egan, and Muegge); two or more of them with "YES" can be regarded as active components. Second, SwissTarget Prediction platform (http://www.swisstargetprediction.ch/) was applied to predict possible targets. SwissTarget Prediction selected the targets whose bioavailability score (BS) was more than 0.85 in the prediction results for further analysis. At the same time, experimentally verified targets information was downloaded from SwissTarget Prediction, and the entries related to the active components of *L. edodes* and *L. decastes* were extracted. Finally, target information was integrated and accumulated to obtain the possible targets of *L. edodes* and *L. decastes* active components.

Prediction o targets of two diseases

Data for all-associated disease targets were acquired from the GeneCards (https://www.genecards.org/) database and Biotechnology Information database (https://www.ncbi.nlm.nih.gov/) (National Center for Biotechnology Information [NCBI]) using "Immune system diseases," "Cancer diseases" and their synonyms. The above targets were converted and queried into the UniProt ID format with "Homo sapiens" as the qualifying condition in the UniProt database. Finally, the gene library of all targets was established by eliminating repeated targets.

Intersection between active compounds and disease targets

The intersection targets between the disease genes and the predicted *L. edodes* and *L. decastes* targets were obtained. Jvenn website (https://jvenn.toulouse.inra.fr/app/example.html) was used to construct a Venn diagram for visualization.

Protein–protein interaction network construction

The above intersection targets were imported into the STRING database (http://string-db.org) for protein interaction network analysis. The screening condition of the species was set to "Homo sapiens" and the minimum required interaction score was "highest confidence (0.9)." Input protein–protein interaction (PPI) information into Cytoscape 3.10.1 for visualization and constructs network of potential key targets.

Topological and cluster analyses of the protein–protein interaction network

The CytoHubba plugin in Cytoscape (https://www.cytoscape.org/) was used to identify hub genes. Three critical topological parameters were chosen for screening core composite targets based on the PPI network: degree, betweenness, and closeness. Values for the three parameters indicated the significance as well as the impact of relevant nodes in the entire network. The MCODE plug-in in Cytoscape was used to screen PPI network modules using various cut-offs: betweenness centrality, betweenness centrality, and degree are greater than the median.

Gene ontology and Kyoto encyclopedia of genes and genomes enrichment analyses

The above-mentioned intersection targets were subjected to the gene ontology (GO) biological process analysis and the Kyoto Encyclopedia of Genes and Genomes (KEGG) pathways enrichment analyses using the DAVID database (https://david.ncifcrf.gov/). R version 3.10.1 was used to visualize the results.

Construction of active compound-target network

For visualization, potential active components and matching intersection targets were imported into the Cytoscape 3.10.1 software and a network of compound-target network was built. Each component of targets is represented by nodes, and the relationship between the components, diseases, and targets is represented by connecting lines.

Culture of cells

Macrophages RAW264.7 and liver cancer cells HepG-2 were cultured. Macrophage RAW264.7 cells were cultured in a constant temperature incubator using a prepared complete medium (DMEM containing 10% fetal bovine serum [FBS] and 1% penicillin/streptomycin). After 48 h of cell culture, the cells adhered to the wall and grew into a monolayer of cells before passage. During passage, the culture medium was discarded, 1 mL of sterile PBS was added to wash twice and then the PBS was discarded. Complete medium, 1 mL, was used to blow until the cells no longer adhered to the wall, and then added to the culture flask containing 6 mL of complete medium prepared in advance. The difference between HepG-2 culture and RAW 264.7 is that the complete culture medium contains 15% FBS and 1% penicillin/streptomycin, and trypsin digestion is required during sub-culturing.

Determination of cell viability

The proliferation and phagocytic proportions of RAW264.7 and the inhibition proportion of HepG-2 were measured. The proliferation and inhibition proportions were determined as follows: (Formula 1), after freeze-drying, a certain amount of DMEM was added to prepare the mother solution, and after ultrasonication, the mother solution was filtered through a 0.22-μm microporous filter membrane for sterilization, and the DMEM was added continuously to dilute the mother solution to obtain different concentrations. RAW264.7 or HepG-2 in the logarithmic growth phase were inoculated on a 96-well plate at a density of 1×10^5/mL, 200 μL per well; the culture medium was discarded after 24 h of culture, and 200 μL of culture medium solution of different

groups was added for 24 h. Using the CCK-8 kit, 20 μL of CCK-8 solution was added to each well and incubated for 1 h, and the absorbance value was measured at 450 nm using an enzyme-linked-immunosorbent serologic assay (ELISA) reader:

$$\frac{\text{Proliferation rate}}{\text{phagocytosis rate}} = \frac{A_1}{A_0} \times 100 \quad (1)$$

The difference in determining phagocytosis rate is that the above CCK-8 kit is replaced with a neutral red kit (Formula 2):

$$\text{Inhibition rate} = \left(1 - \frac{A_1}{A_0}\right) h \quad (2)$$

Statistical analysis

Data were mainly obtained by downloading from public databases. In the cell experiments, each sample with different concentrations was repeated for six times to avoid accidental errors. Data were considered statistically significant with $P < 0.05$.

Results

Targeted analysis of chemical components in *L. edodes* and *L. decastes*

The mass spectrometry results of both fungi were analyzed and compared with the database, which had 120 components of *L. edodes* and 144 components of *L. decastes* (Supplementary Tables S1 and S2 and Supplementary Figure S1). The components with higher contents in the two extracts were carbohydrates, proteins, and fatty acids. Among them, carbohydrates in *L. edodes* accounted for 22.1% and proteins for 16.1%. Carbohydrates in *L. decastes* accounted for 22.4% and proteins 17.3%. The contents of proteins and polysaccharide were the same as reported in edible fungi (Zhou *et al.*, 2023). In addition, *L. edodes* had a higher content of purine and *L. decastes* had a higher content of some organic bases (Figure 1).

Analysis of biological activities of *L. edodes* and *L. decastes*

As raw materials of functional foods, *L. edodes* and *L. decastes* are always consumed wholly. They have complex systems with many types of components; hence, the bioactivity evaluation and mechanism study of a single component cannot truly reflect the overall physiological effects of *L. edodes* and *L. decastes* (Zhang *et al.*, 2022). Here, the potential bioactivity of both fungi was systematically predicted by enrichment analysis of their active components and their corresponding targets (Figure 2). SwissADME web tool database was used to screen and evaluate gastrointestinal absorption and their drug-like properties. This led to the identification of 60 types of medicinal components in *L. edodes* and 73 types in *L. decastes* that met the identification conditions. Further, medicinal components with a bioavailability > 0.85 were selected for further screening, resulting in seven key medicinal components in *L. edodes* and nine in *L. decastes* (Table 3). Many types of fatty acids among key medicinal components were screened. Fatty acids have beneficial health effects, particularly in the prevention of cardiovascular diseases, inflammation, and metabolic disorders, such as diabetes (Coudray *et al.*, 2021). Fatty acids exert significant immune activity by modulating immune cells and regulating intestinal flora (Sganzerla *et al.*, 2022).

In addition, potential targets that satisfied the conditions were obtained. After merging and de-duplicating the potential targets predicted by SwissTarget Prediction,

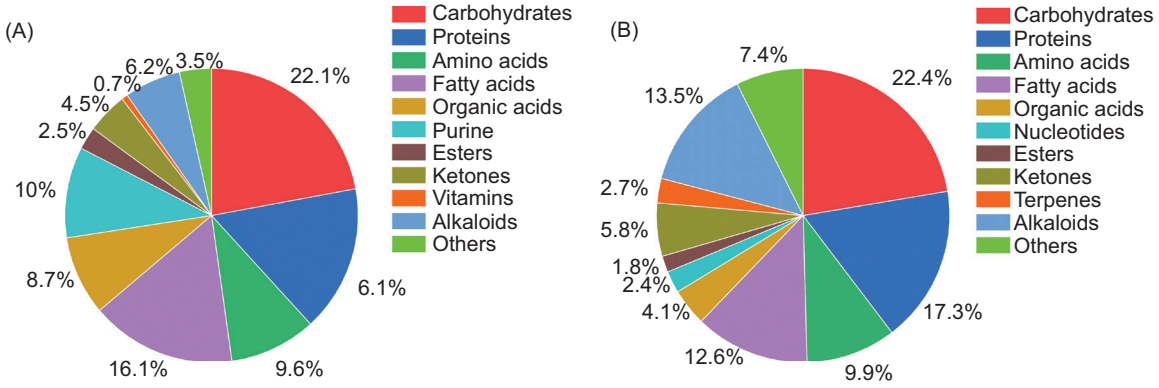

Figure 1. Component content identified by UPLC-Q–TOF-MS. (A) Components of *L. edodes* and (B) components of *L. decastes*.

a total number of *L. edodes* and *L. decastes* targets were calculated, yielding 383 therapeutic targets for key medicinal components of *L. edodes* and 364 therapeutic targets for key medicinal components of *L. decastes.* After collating and removing duplicates, 1,978 ISD gene targets and 1,855 CD gene targets were identified. Through jvenn website, 31 types of intersection targets between *L. edodes* and ISD were discovered, while 27 types associated with CD were also identified. Similarly, 34 types of intersection targets between *L. decastes* and ISD were established, while 25 types associated with CD were also identified. The related targets of these two diseases were queried from GeneCards database and NCBI (Figure 2).

Components act on multiple targets to treat diseases. In general, the components of *L. edodes* and *L. decastes*

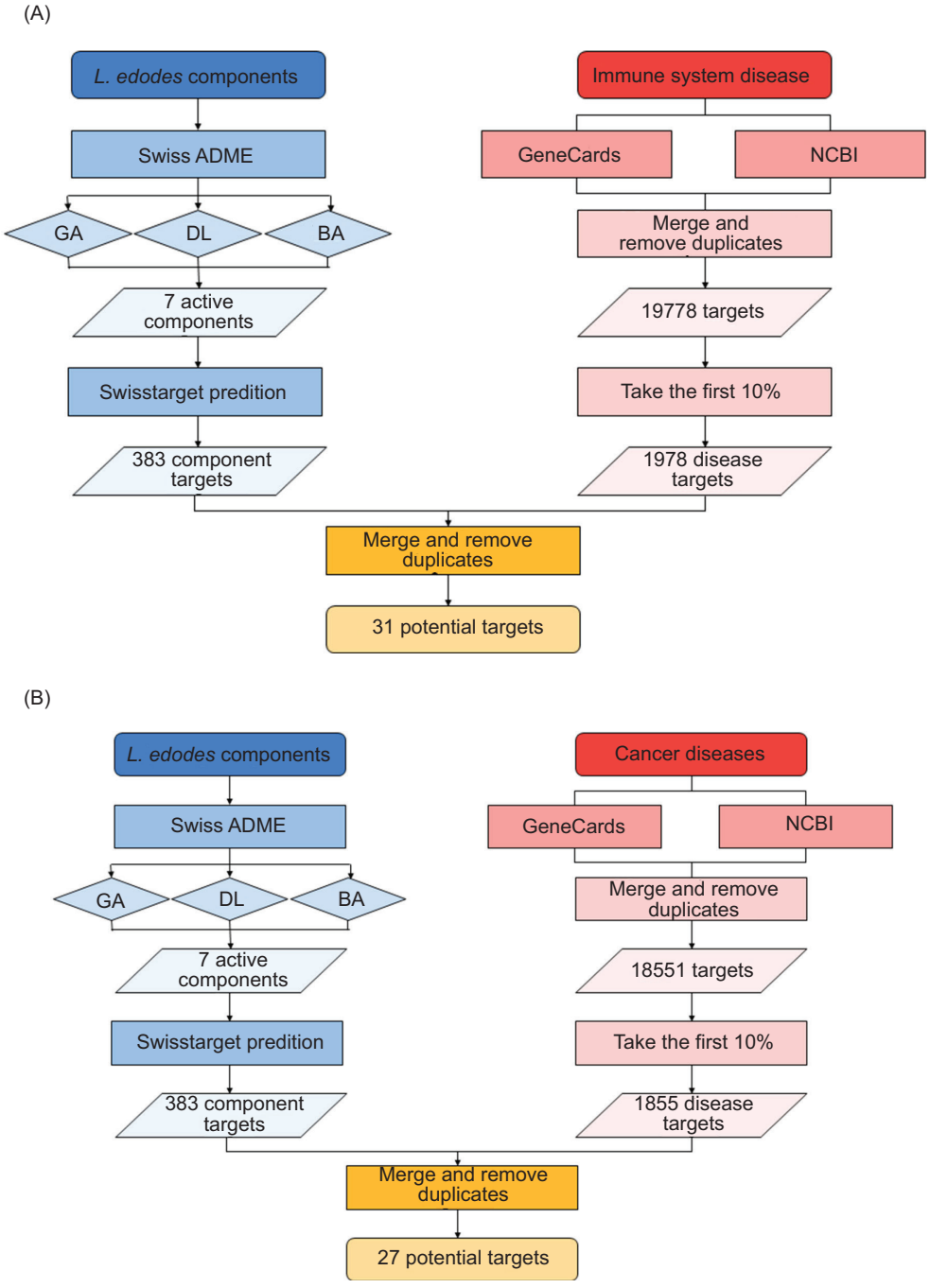

Figure 2. Flow chart for the prediction of targets of active components from fungi and diseases by network pharmacological analysis. (A) Active components of *L. edodes* and ISD; (B) active components of *L. edodes* and CD.

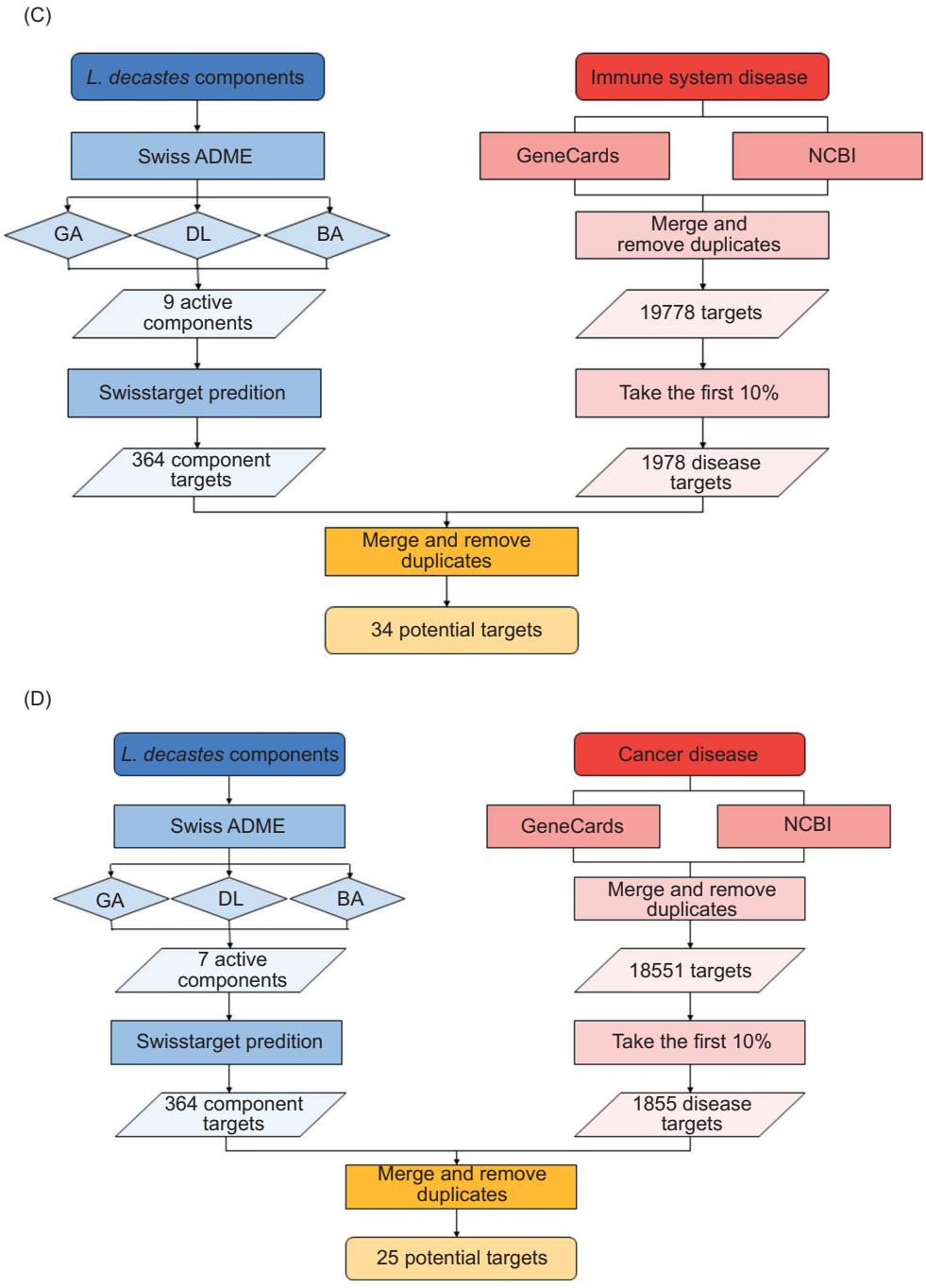

Figure 2. Flow chart for the prediction of targets of active components from fungi and diseases by network pharmacological analysis. (C) active components of *L. decastes* and ISD; and (D) active components of *L. decastes* and CD.

act on 12 targets, such as glycogen synthase kinase 3 beta (*GSK3B*), telomerase reverse transcriptase (*TERT*), and AKT serine/threonine kinase (*AKT1*), for immune regulation, and 13 targets, such as kinase insert domain receptor (*KDR*), peroxisome proliferator-activated receptor alpha (*PPARA*), androgen receptor (*AR*), etc., to affect liver tumors. For example, tryptophan 2,3-dioxygenase 2 can upregulate IL-8 by phosphorylating *AKT–GSK3B* and promote the polarization of M2 macrophages. The activation of peroxisome proliferator-activated receptor gamma (*PPARG*) can regulate the cell cycle distribution of colon cancer cells and promote cell apoptosis (Selenz *et al.*, 2022). In addition, the two edible fungi components can simultaneously act on 10 targets, such as *GSK3B*, *AKT1*, and *PTGS2*, to affect immune function and liver tumor development. This shows that some targets play a wide range of roles when participating in biological activities, which could be a key point in disease regulation.

Table 3. Active components of *L. edodes* and *L. decastes*.

L. edodes		*L. decastes*	
No.	**Active components**	**No.**	**Active components**
1.	FA 18:2+2O	1.	FA 18:2+2O
2.	L-5-Oxoproline	2.	FA 18:3+2O
3.	Propanoic acid	3.	FA 18:1+1O
4.	FA 18:4+2O	4.	Succinic acid
5.	Lapachol	5.	9Z,12Z-linoleic acid
6.	Sebacic acid	6.	Maleic acid
7.	10-Hydroxydecanoic acid	7.	16-Hydroxyhexadecanoic acid
		8.	3-Methyladipic acid
		9.	Ketoisovaleric acid

Gene set enrichment analysis of GO and KEGG

Finally, further enrichment analysis was conducted to analyze overlapping targets and the detailed results. Similar to the results obtained for the targets, several identical GO biological processes and KEGG pathways were observed in the first four panels (Figure 4), indicating that these represent key biological processes and pathways for treatment of diseases by fungi. Enrichment analysis of seven active components of *L. edodes* yielded 31 core targets related to immunity. In all, 309 GO biological processes, 99 KEGG signaling pathways and 27 core targets related to cancer were obtained. Enrichment analysis of 305 GO biological processes and 96 KEGG signaling pathways were obtained. Correspondingly,

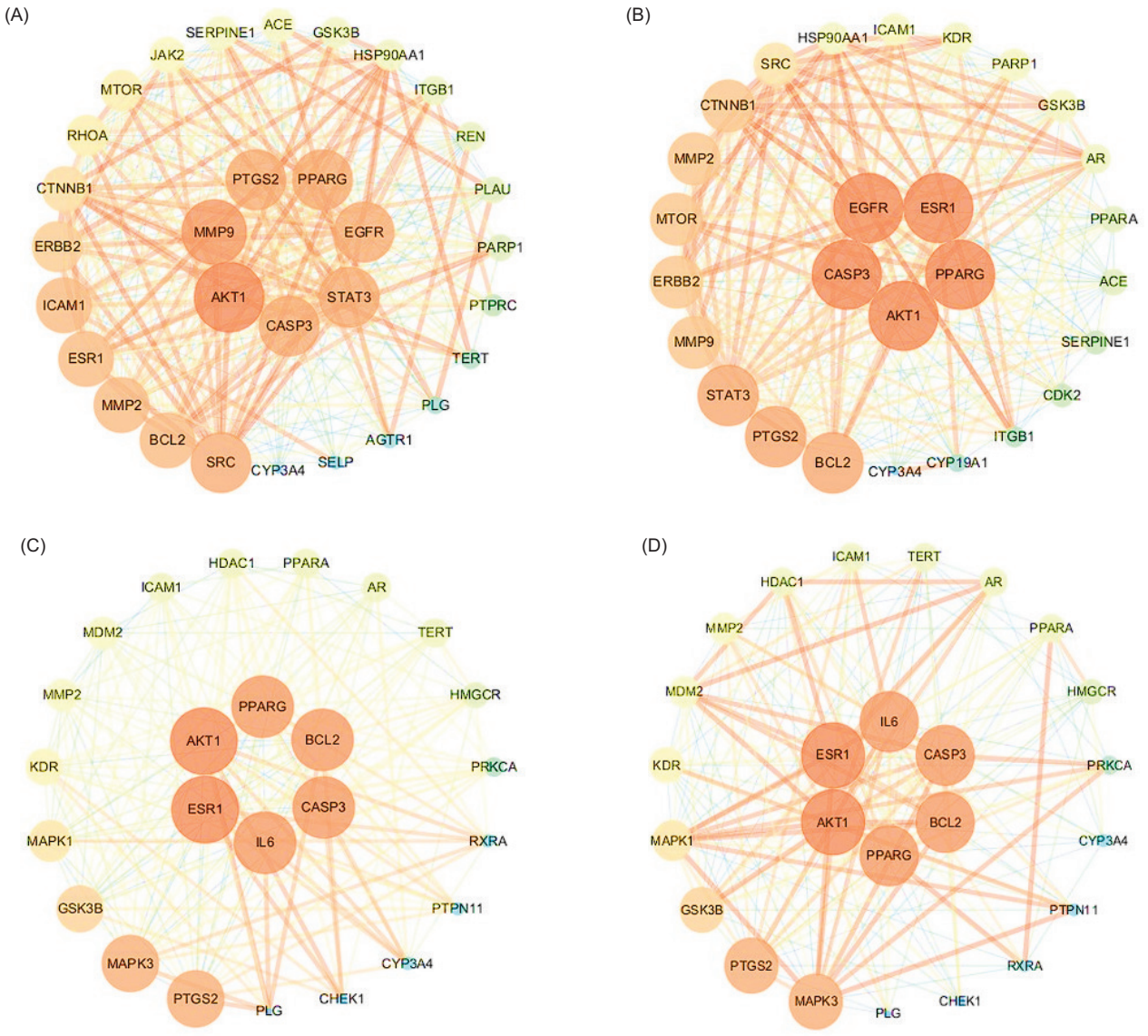

Figure 3. Interaction network diagram of core pharmacodynamic targets of fungi components for treating diseases. (A) *L. edodes* components and ISD; (B) *L. edodes* components and CD; (C) *L. decastes* components and ISD; and (D) *L. decastes* components and CD.

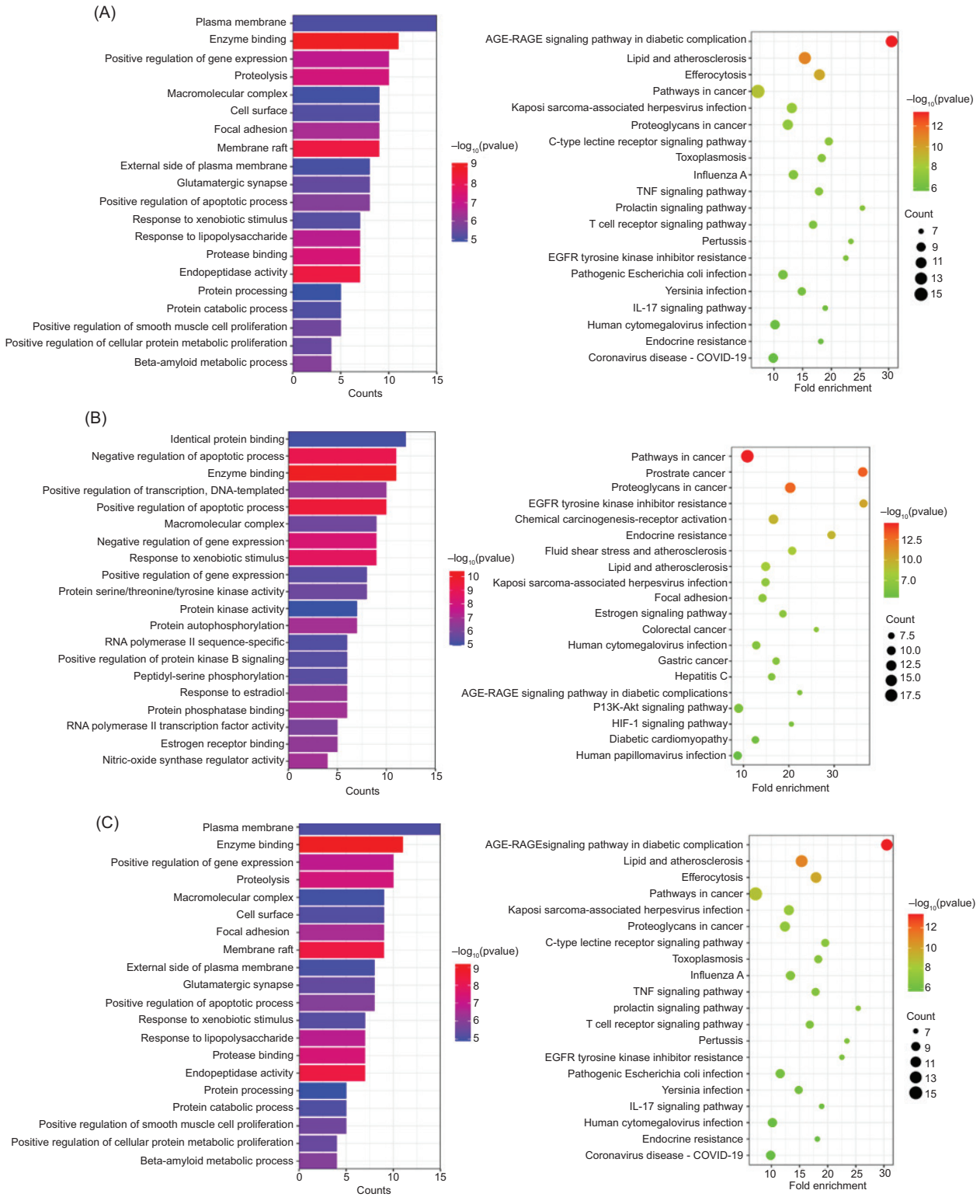

Figure 4. The GO and KEGG enrichment analysis of core pharmacodynamic targets. (A) *L. edodes* components and ISD; (B) *L. edodes* components and CD; (C) *L. decastes* components and ISD.

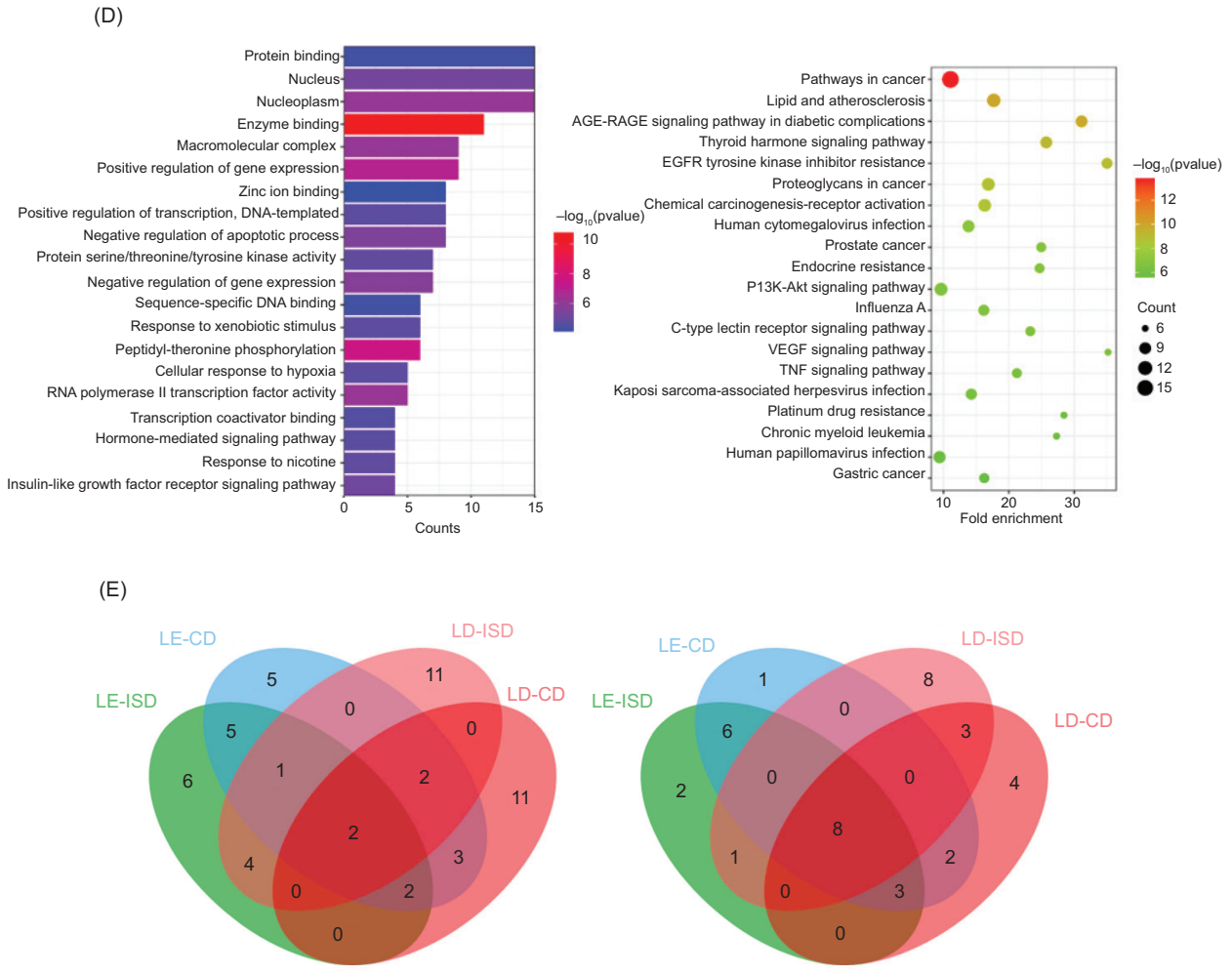

Figure 4. The GO and KEGG enrichment analysis of core pharmacodynamic targets. (D) *L. decastes* components and CD; and (E) Venn diagram of the results of enrichment analysis of the intersection of components and diseases. The results of GO analysis are on the left and that of KEGG analysis on the right.

enrichment analysis of nine types of active components of *L. decastes* yielded 34 core targets related to immunity, and 300 GO biological processes, 135 KEGG signaling pathways, and 25 core targets related to cancer. Enrichment analysis resulted in 218 GO biological processes and 137 KEGG signaling pathways.

For two diseases, the GO enrichment analysis revealed that the targets of *L. edodes* were always closely related to 10 biological processes, which were nitric oxide (NO) synthase regulator activity, protein phosphatase binding, protein autophosphorylation, positive regulation of protein kinase B signaling, estrogen receptor binding, positive regulation of apoptotic process, enzyme binding, response to xenobiotic stimulus, negative regulation of gene expression, and negative regulation of apoptotic process, The KEGG pathway enrichment analysis indicated that the targets of *L. edodes* were always significantly enriched in 17 pathways, which were prostate cancer, colorectal cancer, fluid shear stress and atherosclerosis, chemical carcinogenesis–receptor activation, diabetic cardiomyopathy, focal adhesion, estrogen signaling pathway, gastric cancer, HIF-1 signaling pathway, pathways in cancer, proteoglycans in cancer, lipid and atherosclerosis, epidermal growth factor receptor (EGFR) tyrosine kinase inhibitor resistance, endocrine resistance, advanced glycation endproducts–receptor for advanced glycation endproducts (AGE-RAGE) signaling pathway in diabetic complications, Kaposi sarcoma-associated herpesvirus infection, and human cytomegalovirus infection. Likewise, for two diseases, the GO enrichment analysis showed that the targets of *L. decastes* were always closely related to four biological processes, which were enzyme binding, response to xenobiotic stimulus, macromolecular complex and positive regulation of gene expression. The KEGG pathway enrichment analysis indicated that the targets of *L. decastes* were always significantly enriched in nine pathways, which were pathways in cancer, proteoglycans in cancer, lipid and atherosclerosis, EGFR tyrosine kinase inhibitor resistance, endocrine

resistance, AGE-RAGE signaling pathway in diabetic complications, Kaposi sarcoma-associated herpesvirus infection, human cytomegalovirus infection, and prolactin signaling pathway.

Components–targets–pathways–diseases network analysis

The "components–targets–pathways–diseases" network analysis diagram illustrates the interplay between various elements (Figure 4). Yellow rectangles denote biological processes or signaling pathways, blue rectangles represent key targets associated with these pathways, red diamonds depict potential active components, and green ovals indicate diseases. This figure serves to elucidate the intricate relations among these components and their relevance to disease pathogenesis. It can be seen that the potential active components, such as octadecadienoic acid, octadecatrienoic acid, and lapachol in *L. edodes*, can act on 22 targets, such as *PARP1*, *CTNNB1*, and steroid receptor coactivator (*SRC*), to regulate pathways in cancer. EGFR tyrosine kinase inhibitor and other signaling pathways produce immune and tumor suppressive effects (Figure 5A). Similarly, potential active ingredients, such as octadecadienoic acid, octadecenoic acid, and linoleic acid

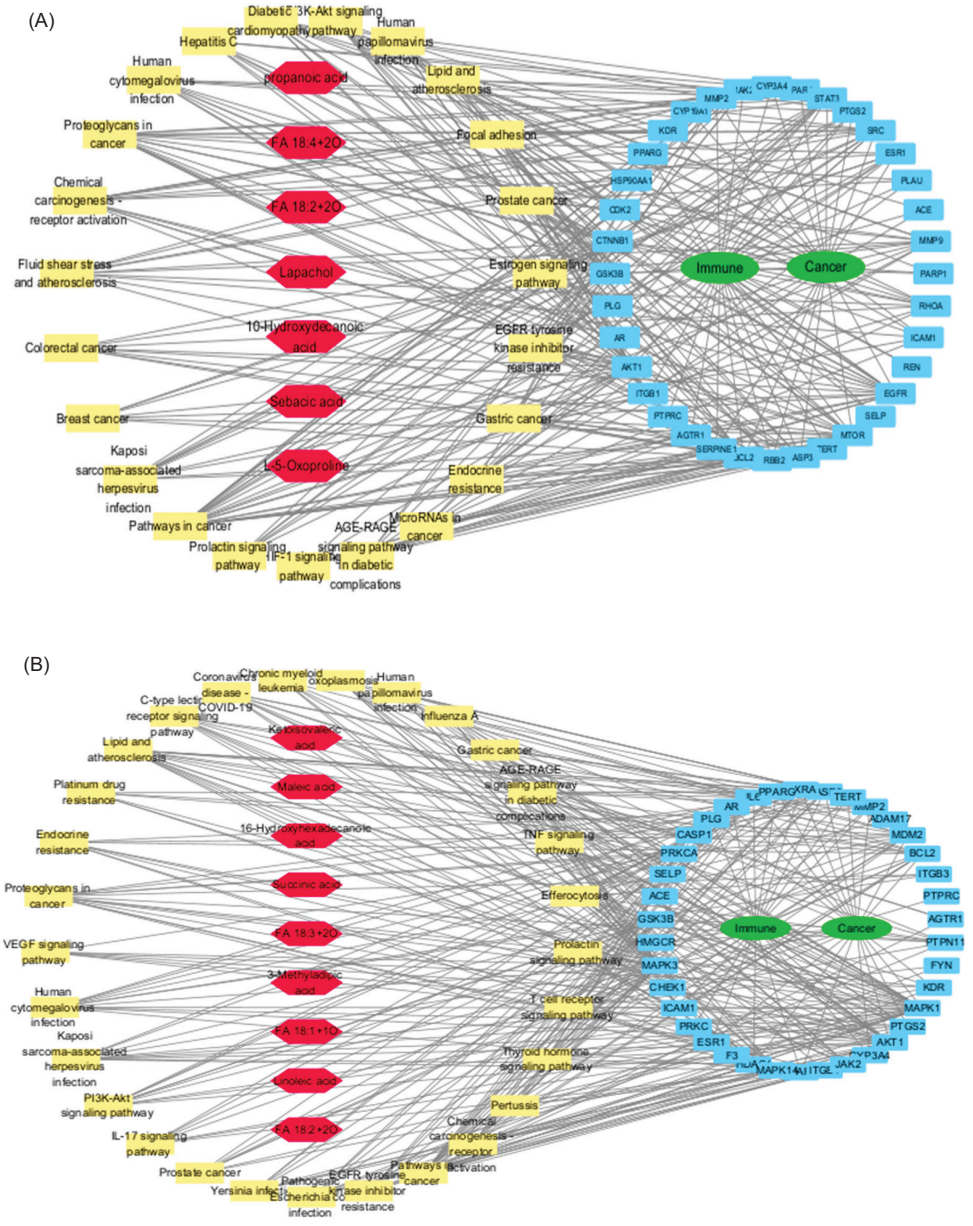

Figure 5. Components–targets–pathways–diseases network analysis. (A) *L. edodes* components and two diseases and (B) *L. decastes* components and two diseases.

in *L. decastes*, can act on 13 targets, such as *GSK3B*, *AKT1*, and *PTGS2* points, and then regulate signaling pathways, such as pathways in cancer, EGFR tyrosine kinase inhibitor, AGE-RAGE signaling pathway, etc., to produce immune and tumor suppressive effects (Figure 5B).

Cell experiment verification

The cell proliferation rate or phagocytosis rate of blank control group was defined as 100%. Changes in the proliferation and phagocytosis of macrophages of RAW264.7 were studied. The results showed significant differences in cell proliferation and phagocytosis between the experimental group and the control group. In addition, dosage differences were observed between different concentrations. At appropriate concentrations, edible fungi have a significant stimulating effect on macrophages, significantly promoting their growth and activity (Figures 6A and 6B). Similarly, as concentration increased, the toxicity of edible fungi to HepG-2 became stronger, with a clear effect of inhibiting cell growth (Figure 6C).

Discussion

Modern studies on the composition and pharmacological activity of *L. edodes* and *L. decastes* mostly focused on single component and single activity, which seriously interfered the development and utilization of *L. edodes* and *L. decastes*. Traditional Chinese medicine emphasizes the holistic concept, and its drug use has the characteristics of multi-target and multi-function. Furthermore, various pieces of evidence suggest that targets, biological processes, and metabolic pathways play important roles in diseases. In our study, we used the PPI network to construct network targets for fungi and diseases from a holistic and systemic perspective for further screening core genes. Subsequently, we explored their potential mechanisms of action through GO and KEGG enrichment analysis. Finally, we utilized the component–target–pathway-disease network to unveil the mechanism through which its components influenced targets, regulated target pathways or biological processes, and consequently treated diseases.

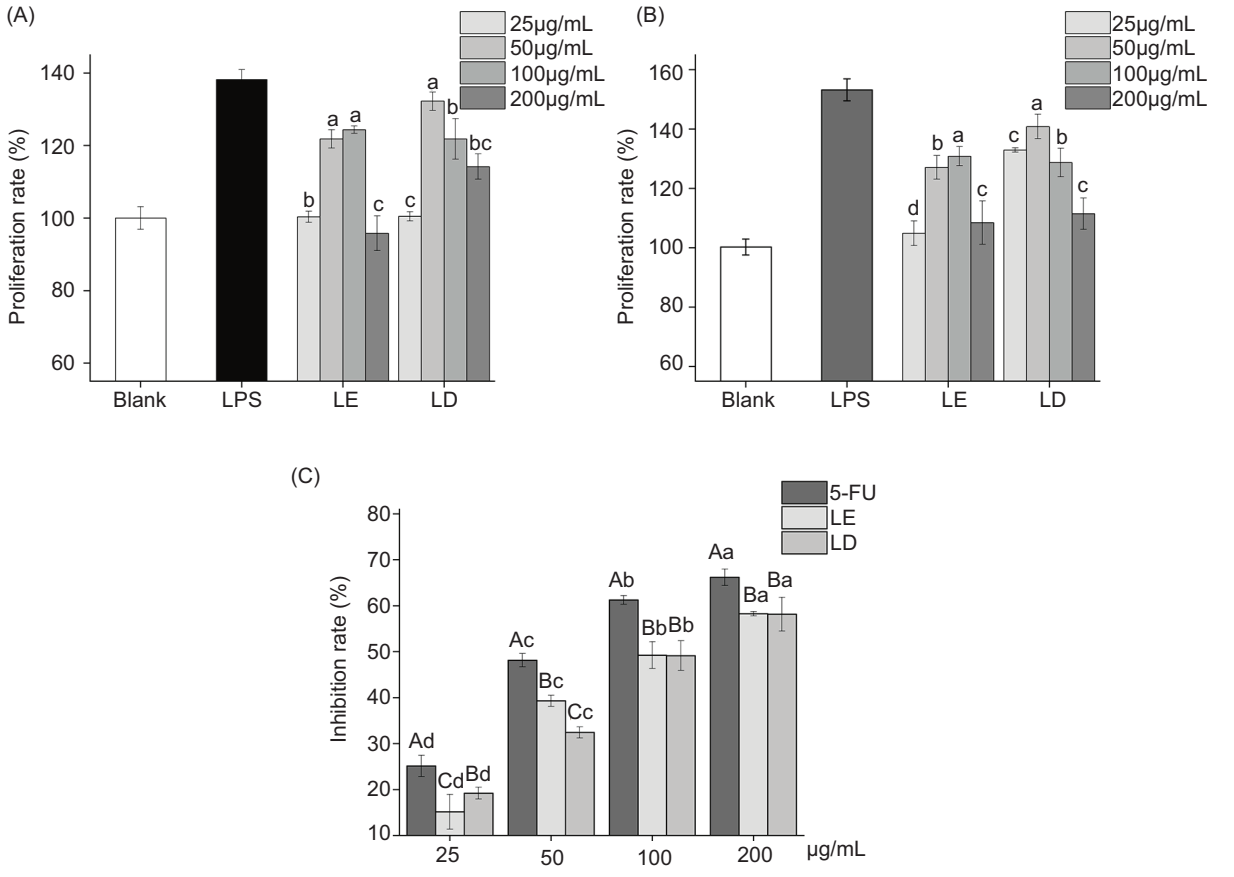

Figure 6. Changes in the activity of different cells after edible fungi treatment. (A) Changes in RAW264.7 proliferation rate; (B) changes in RAW264.7 phagocytosis rate and (C) changes in HepG-2 inhibition rate. Lowercase letters represent significant differences between different concentrations in the same group, and uppercase letters represent significant differences between different groups at the same concentration (n = 6, *P* < 0.05).

First, we discussed several targets of interest. AKT1, also known as protein kinase B, is an important member of mitogen-activated protein kinase that exerts a key role in cell signaling. It serves as one of the central components of the PI3K/AKT signaling pathway and is involved in regulating a variety of biological processes, such as cell growth, proliferation, survival, and metabolism (Guerau-Arellano *et al.*, 2022). Within the immune system, AKT1 is involved in cell proliferation, differentiation, and survival of T and B cells, and its activation may promote immune cell functions. AKT1 modulated adaptive immune response of Nile tilapia by promoting lymphocyte activation and proliferation via mammalian target of rapamycin complex 1 (mTORC1) signaling (Ai *et al.*, 2021). In cancer, aberrant activation of AKT1 occurs, and its activation may promote tumor cell proliferation, survival, and invasion and inhibits apoptosis, rendering it a potential therapeutic target. For example, Yang *et al.* (2022) demonstrated that inhibition of AKT1 suppresses the growth of prostate cancer cells.

PPARG is a nuclear receptor that acts as a transcription factor and is widely distributed in a variety of tissues, such as adipose tissue, liver, intestine, and immune cells, in the human body (Rudko *et al.*, 2020). Within the immune system, PPARG is involved in regulating inflammatory response, cell migration, and phagocytosis in the monocyte–macrophage system. Studies demonstrated that PPARG could be employed to temper allergic inflammation by suppressing pro-inflammatory gene expression programs in epithelial cells (Stark *et al.*, 2021). In addition, many synthetic agonists of PPARG are shown to suppress hepatocellular carcinoma (HCC); these synthetic agonists prevent HCC invasion and metastasis by inducing cell cycle arrest and apoptosis in HCC cells (Katoch *et al.*, 2022).

In addition to several shared pathways, there are also specific targets directed by components for treating diseases. For instance, protein tyrosine phosphatase receptor type C (*PTPRC*) is identified as the target modulated by *L. edodes* in the treatment of ISD. The *PTPRC* gene, also known as the *CD45* gene, encodes a phosphatase located on the cell membrane. Immune-related genes, such as *CD45* and *CD69*, exhibit activation in hyperimmune subtype group of chronic kidney disease (CKD), leading to a higher proportion of immune cells. This finding holds promising implications for the treatment of CKD (Fang *et al.*, 2024). Similarly, the protein kinase C alpha (*PRKCA*) target gene is affected by *L. decastes* in the treatment of CKD. *PRKCA* encodes the protein kinase C alpha. The circular(circ)-*PRKCA* promotes the tumorigenesis of non-small cell lung cancer (NSCLC). Xu *et al.* (2021) demonstrated that curcumin inhibits the growth of NSCLC by downregulating circ-*PRKCA*.

Second, we discussed various important pathways of interest. EGFR tyrosine kinase inhibitor resistance is the most significant pathway of fold enrichment. EGFR, the receptor for members of the epidermal growth factor family, regulates cell proliferation and signal transduction. Moreover, EGFR is associated with inhibiting cell proliferation, angiogenesis, invasion, metastasis, and apoptosis. Therefore, EGFR has emerged as an important target for the treatment of cancer, including NSCLC, head and neck cancers, breast cancer, glioma, cervical cancer, and bladder cancer (Shi *et al.*, 2022). The EGFR signaling pathway regulates proliferation, migration, and cytokine secretion of immune cells, thereby impacting the activity and functioning of immune cells. The inhibition of EGFR mediates the activation of immune cells and enhances the local proliferation of T cells in the environment (Zou *et al.*, 2020). EGFR inhibitors block cell proliferation, metastasis, and other signaling pathways by inhibiting EGFR tyrosine kinase activity, thereby inhibiting the growth of cancer cells. Upon activation, EGFR triggers multiple downstream signaling pathways, such as PI3K/AKT and mitogen-activated protein kinase (MAPK) pathways, to promote cell growth. Proliferation, survival, and metastasis thereby promote the increased activity of immune cells (Selenz *et al.*, 2022).

The MAPK pathway is an important signaling pathway. It plays a key regulatory role in cells and is involved in the regulation of various biological processes, such as cell proliferation, apoptosis, cell differentiation, cell migration, and inflammation. MAPKs are one of the most important enzymes in various cellular activities and involve a series of phosphorylation reactions. They are activated through receptors on cell membranes, respond to external signals, and regulate cell growth, differentiation, apoptosis, stress, and other processes (Kim *et al.*, 2018). The MAPK family involves most of the pathways and mediates the activation process of immune cells, such as macrophages, T cells, and B cells. When cells are stimulated by external stimuli, such as bacterial and viral infection or cytokine stimulation, the MAPK pathway is activated, thereby triggering the corresponding response of the cell (Vilela *et al.*, 2010). Both MAPK1 and MAPK3 belong to the mitogen-activated protein kinase family and promote the proliferation as well as inhibition of the apoptosis of cancer cells. Lee *et al.* (2022) used the inRas37 antibody, a KRAS-targeting antibody, to increase significantly the drug response of dual inhibitor BEZ-235 (also known as NVP-BEZ235 or RTB101) against pancreatic cancer cells by inhibiting MAPK.

In addition to several shared pathways, specific pathways targeted by components for treating diseases are also studied. The biological process involving most of the genes in the treatment of CD by *L. edodes* is

identical protein binding, which refers to the process in which two or more identical proteins bind to each other to form a complex, and the binding of certain identical proteins may alter the transcription, translation, or stability of oncogenes, thus affecting the functioning of relevant genes. Wei *et al*. (2022) found that cancer cells often show resistance to drugs, and that the binding of the same proteins regulates relevant signaling pathways, affecting the sensitivity of cancer cells to therapeutic drugs, and thus affecting the treatment of cancer. The AGE-RAGE signaling pathway is the signaling pathway with the smallest *P*-value and the largest enrichment index in the treatment of ISD by *L. decastes.* The activation of AGE-RAGE signaling pathway induces the production of cytokines, such as TNF-α and IL-6, which are able to activate immune cells. The pathway also plays a key role in the maintenance of immune tolerance and suppression of immune response by influencing the functioning and number of immune cells, including regulatory T-cells (Sukjamnong *et al.*, 2022).

Finally, we discussed the "components–targets–pathways–diseases" network. It was indicated that *L. edodes* and *L. decastes* had potential effect on regulating overlapping targets and multiple pathways, thus serving as a latent multi-target and multi-pathway treatment for two mentioned diseases. It is observed that seven active components of *L. edodes* and nine active components of *L. decastes* act on common targets, such as AKT1 and PPARG, thereby regulating signal pathways, such as EGFR and MAPK, to affect the body, and have immunomodulatory and liver tumor inhibition effects. The results showed that the mechanism of action of two fungi includes maintaining autoimmune tolerance and preventing normal tissues from being attacked by the immune system. External signal molecules can bind to receptors or signal molecules on cell membrane, triggering the activation and functional regulation of immune cells (Zhang *et al.*, 2021). SRC regulates the activity of immune cells by affecting signal transduction, such as regulating the phosphorylation state of cytoskeleton (Chen *et al.*, 2023) as well as inhibiting signaling pathways to enhance the immune response ability of immune cells and enhancing the immune system's ability to attack tumor cells. EGFR signaling pathways inhibition mediates immune cell activation and increases local proliferation of T cells in the tumor environment (Halder *et al.*, 2023). Therefore, the combined application of tumor suppressor drugs and immunotherapy drugs has a synergistic effect on cancer treatment. Shin *et al.* (2016) used an EGFR tyrosine kinase inhibitor and a PD-1 inhibitor, in combined application, blocking the combination of PD-1 and PD-L1 to inhibit the signaling pathway and enhance the killing ability of immune cells against tumor cells.

Conclusions

This study identified key bioactive components in *L. edodes* and *L. decastes* with potential immuno-enhancing and anticancer properties. It also explored the mechanisms of how active components exert their effects. The therapeutic mechanisms of *L. edodes* and *L. decastes* for immune system diseases include maintaining autoimmune tolerance, preventing normal tissues from being attacked by the immune system, inhibiting signal pathways, and enhancing the immune response of immune cells. On the other hand, the therapeutic mechanisms for liver cancer include inhibiting the activation of mitogen-activated proteins, blocking the EGFR pathway, and inhibiting the growth and metastasis of cancer cells. In addition, edible fungi also play both immunomodulatory and liver tumor inhibition roles. It was observed that enhancing body's immune response is an important way to treat cancer. These findings serve as a crucial reference for elucidating the biological activities of *L. edodes* and *L. decastes*, and predict mechanisms of drug action. Activity verification in cell experiments also confirmed our analysis. It is recommended to explore the clinical applications of these bioactive ingredients and their mechanisms of action in more detail.

Data Availability Statement

Data are available upon request.

Author Contributions

Yingnan Zhang: conceptualization, data curation, investigation, formal analysis, writing of original draft. Gaoxing Ma: writing, review and editing as well as supervision. Fei Pei: writing, review and editing, and software application. Ning Ma: writing, review and editing as well as visualization. Anxiang Su: writing, review and editing as well as validation. Qiuhui Hu: conceptualization, methodology, fund acquisition, and project administration. Meng Wang: conceptualization, methodology, formal analysis, writing of original draft, and review and editing.

Conflicts of Interest

The authors declared that they had no known competing financial interests or personal relationships that could have influenced this paper.

Funding

This research was funded by Jiangsu Province Agricultural Science and Technology Innovation Fund (CX(21)2005).

References

Ai, K.T., Yan, J., Li, K., et al., 2021. Akt1/mTORC1 signaling modulates adaptive immune response of Nile tilapia by promoting lymphocyte activation and proliferation. Developmental and Comparative Immunology 119: 10. https://doi.org/10.1016/j.dci.2021.104042

Chen, K., Dai, M.X., Luo, Q.N., et al., 2023. PARP1 controls the transcription of CD24 by ADP-ribosylating the RNA helicase DDX5 in pancreatic cancer. International Journal of Biochemistry – Cell Biology 155: 11. https://doi.org/10.1016/j.biocel.2022.106358

Coudray, C., Durand, E., Balas, L., et al., 2021. Potential favourable health effects of some dietary uncommon fatty acids. Ocl-Oilseeds and Fats Crops and Lipids 28(41): 9. https://doi.org/10.1051/ocl/2021028

Cui, L., Liu, Y., Liu, M., et al., 2022. Identification of phytochemicals from *Lentinus edodes* and *Auricularia auricula* with UPLC-Q-Exactive Orbitrap MS. Journal of Future Foods 2(3): 253–260. https://doi.org/10.1016/j.jfutfo.2022.06.006

Dai, J.N., Liu, B.L., Ji, D., et al., 2023a. Extraction, isolation, identification, and bioactivity of polysaccharides from Antrodia cinnamomea. Quality Assurance and Safety of Crops – Foods 15(4): 60–76. https://doi.org/10.15586/qas.v15i4.1341

Dai, Y., Wang, L., Chen, X.Y., et al., 2023b. *Lentinula edodes*sing polysaccharide: extraction, characterization, bioactivities, and emulsifying applications. Foods 12(17): 17. https://doi.org/10.3390/foods12173289

Ding, X., Liu, Y. and Hou, Y. L., 2022. Structure identification and biological activities of a new polysaccharide isolated from *Lyophyllum decastes (Fr.) Sing.* Pharmacognosy Magazine 18(77): 112–120. https://doi10.4103/pm.pm_185_21

Du, Y.H., Zhao, J.J., Li, X., et al., 2024. Mechanism of pachymic acid in the treatment of gastric cancer based on network pharmacology and experimental verification. World Journal of Gastrointestinal Oncology 16(1): 22. https://10.4251/wjgo.v16.i1.30

Fang, X.D., Chen, Y.X., Chen, Y., et al., 2024. Identification and characterization of two immune-related subtypes in human chronic kidney disease. Transplant Immunology 82: 10. https://doi.org/10.1016/j.trim.2023.101983

Fujita, R., Yokono, M., Ube, N., et al., 2021. Suppression of *alternaria brassicicola* infection by volatile compounds from spent mushroom substrates. Journal of Bioscience and Bioengineering 132(1): 25–32. https://doi10.1016/j.jbiosc.2021.03.003

Gameli-Kwabla, K., 2020. Examining the nutritional composition, value and health benefit of mushrooms. International Journal of Reseach and Scholarly Communication 3(1): 17.

Garcia, J., Rodrigues, F., Saavedra, M.J., et al., 2022. Bioactive polysaccharides from medicinal mushrooms: a review on their isolation, structural characteristics and antitumor activity. Food Bioscience 49: 11. https://doi.org/10.1016/j.fbio.2022.101955

Guerau-Arellano, M., Piedra-Quintero, Z.L.L. and Tsichlis, P.N., 2022. Akt isoforms in the immune system. Frontiers in Immunology 13: 990874. https://doi10.3389/fimmu.2022.990874

Halder, S., Basu, S., Lall, S.P., et al., 2023. Targeting the EGFR signaling pathway in cancer therapy: what's new in 2023? Expert Opinion on Therapeutic Targets 27(4–5): 305–324. https://doi.org/10.1080/14728222.2023.2218613

Hye-Lim, J., Park, S.-Y. and Nam, J., 2017. Effect of extraction solvent on the antioxidant activity of *Lentinula edodes* GNA01 extract. Korean Journal of Food and Nutrition 30(1): 51–58. https://doi10.9799/ksfan.2017.30.1.051

Ike, K., Kameyama, N., Ito, A., et al., 2012. Induction of a T-Helper 1 (Th1) immune response in mice by an extract from the *pleurotus eryngii (Eringi)* mushroom. Journal of Medicinal Food 15(12): 1124–1128. https://doi10.1089/jmf.2012.2239

Katoch, S., Sharma, V. and Patial, V., 2022. Peroxisome proliferator-activated receptor gamma as a therapeutic target for hepatocellular carcinoma: experimental and clinical scenarios. World Journal of Gastroenterology 28(28): 21. https://doi10.3748/wjg.v28.i28.3535

Kim, M. and Ryu, S.E., 2018. Specific binding and catalytic activation of the MAPK-MKP complex. Biodesign 6(4): 79–83.

Lee, J.E., Woo, M.G., Jung, K.H., et al., 2022. Combination therapy of the active KRAS-targeting antibody inRas37 and a PI3K inhibitor in pancreatic cancer. Biomolecules and Therapeutics 30(3): 274–283. https://doi10.4062/biomolther.2021.145

Li, H.Y., Guo, L., Ding, X.Y., et al., 2022. Molecular networking, network pharmacology, and molecular docking approaches employed to investigate the changes in ephedrae herba before and after honey-processing. Molecules 27(13): 18. https://doi.org/10.3390/molecules27134057

Li, Y.H., Liu, X.H., Zhang, X., et al., 2021. Immune cycle-based strategies for cancer immunotherapy. Advanced Functional Materials 31(50): 27. https://10.1002/adfm.202107540

Liang, Z., Li, C., Wang, J., et al., 2021. Immunomodulatory effects of polysaccharides from edible fungus: a review. Food Science and Human Wellness 10(4): 393–400. https://doi.org/10.1016/j.fshw.2021.04.001

Lin, M., 2012. Fungi medicine in Chinese materia medica. Chinese Traditional and Herbal Drugs.

Lu, X.S., Hou, H., Fang, D.L., et al., 2022. Identification and characterization of volatile compounds in *Lentinula edodes* during vacuum freeze-drying. Journal of Food Biochemistry 46(6): 13. https://doi10.1111/jfbc.13814

Sharma, A., Bhardwaj, G., Nayik, G.A. 2023. Phytochemistry and nutritional composition of significant wild medicinal and edible mushrooms. eBook collection. Royal Society of Chemistry, London. https://doi10.1039/9781837672097

Qiu, M.Y., Zhang, J.Q., Wei, W.L., et al., 2024. Integrated UPLC/Q-TOF-MS/MS analysis and network pharmacology to reveal the neuroprotective mechanisms and potential pharmacological ingredients of *aurantii fructus immaturus* and *aurantii fructus*. Pharmaceuticals 17(2): 14. https://doi.org/10.3390/ph17020239

Roszczyk, A., Turlo, J., Zagozdzon, R., et al., 2022. Immunomodulatory properties of polysaccharides from *Lentinula edodes*. International Journal of Molecular Sciences 23(16): 13. https://doi10.3390/ijms23168980

Rudko, O.I., Tretiakov, A.V., Naumova, E.A., et al., 2020. Role of PPARs in progression of anxiety: literature analysis and signaling

pathways reconstruction. PPAR Research 2020: 8859017. https://doi10.1155/2020/8859017

Selenz, C., Compes, A., Nill, M., et al., 2022. EGFR inhibition strongly modulates the tumour immune microenvironment in EGFR-Driven non-Small-Cell lung cancer. Cancers 14(16): 15. https://doi10.3390/cancers14163943

Sganzerla, W.G., Todorov, S.D. and da Silva, A.P.G., 2022. Research trends in the study of edible mushroom: nutritional properties and health benefits. International Journal of Medicinal Mushrooms 24(5): 1–18.

Shi, K.Y., Wang, G., Pei, J.P., *et al.*, 2022. Emerging strategies to overcome resistance to third-generation EGFR inhibitors. Journal of Hematology and Oncology 15(1): 44. https://doi10.1186/s13045-022-01311-6

Shin, J.H. and Park, H.-B., 2016. Enhanced anti-tumor reactivity of cytotoxic T lymphocytes expressing PD-1 decoy. Immune Network 16(2): 134–139. https://doi10.4110/in.2016.16.2.134

Stark, J.M., Coquet, J.M. and Tibbitt, C.A., 2021. The role of PPAR-γ in allergic disease. Current Allergy and Asthma Reports 21(11): 8. https://doi10.1007/s11882-021-01022-x

Starzer, A.M., Preusser, M. and Berghoff, A.S., 2022. Immune escape mechanisms and therapeutic approaches in cancer: the cancer-immunity cycle. Therapeutic Advances in Medical Oncology 14: 14. https://10.1177/17588359221096219

Sukjamnong, S., Chen, H., Saad, S., et al., 2022. *Fimbristylisovata* and *artemisia vulgaris* extracts inhibited AGE-mediated RAGE expression, ROS generation, and inflammation in THP-1 cells. Toxicological Research 38(3): 331–343. https://doi10.1007/s43188-021-00114-0

Vilela, B., Pagès, M. and Lumbreras, V., 2010. Regulation of MAPK signaling and cell death by MAPK phosphatase MKP2. Plant Signaling and Behavior 5(11): 1497–1500. https://doi10.4161/psb.5.11.13645

Wang, Y.H., Yang, Z.Y., Chen, X., et al., 2021. Lenthionine, a key flavor substance in *Lentinula edodes*, is regulated by cysteine under drought stress. Journal of Agricultural and Food Chemistry, 69(43): 12645–12653. https://doi10.1021/acs.jafc.1c04829

Wei, A.A.J., Iacobucci, C., Schultze, W., et al., 2022. Different oligomeric states of the tumor suppressor p53 show identical binding behavior towards the S100β homodimer. Chembiochem 23(11): 6. https://doi10.1002/cbic.202100665

Wen, S.D., Mo, S., Zhou, J., et al., 2024. Single-cell and spatial-omics in delineating immune-related diseases. Frontiers in Cell and Developmental Biology 12: 3. https://doi.org/10.3389/fcell.2024.1365242

Xie, Y.M., Shi, L.S., He, X.S., et al., 2021. Gastrointestinal cancers in China, the USA, and Europe. Gastroenterology Report 9(2): 91–104. https://10.1093/gastro/goab010

Xu, L.L., Yang, W.J., Qiu, T.M., et al., 2023. Complete genome sequences and comparative secretomic analysis for the industrially cultivated edible mushroom *Lyophyllum decastes* reveals insights on evolution and lignocellulose degradation potential. Frontiers in Microbiology 14: 14. https://doi10.3389/fmicb.2023.1137162

Xu, X.M., Yu, D.H., Wang, Y., et al., 2024. Integrating network pharmacology and renal metabonomics to reveal the protective mechanism of resveratrol on gouty nephropathy. Biomedical Chromatography 38(5): e5839. https://10.1002/bmc.5839

Xu, X.Q., Zhang, X.Y., Zhang, Y., et al., 2021. Curcumin suppresses the malignancy of non-small cell lung cancer by modulating the circ-PRKCA/miR-384/ITGB1 pathway. Biomedicine & Pharmacotherapy 138: 111439. https://doi.org/10.1016/j.biopha.2021.111439

Yang, M., Liu, H., Qiu, G.P., et al., 2022. Silencing Akt1 enhances the resistance of prostate cancer cells to starvation and inhibits starvation-induced lung metastasis through epithelial-mesenchymal transition in prostate cancer. Medical Oncology 39(1): 12. https://doi10.1007/s12032-021-01600-z

Yin, Z., Sun-Waterhouse, D., Wang, J., et al., 2022. Polysaccharides from edible fungi *Pleurotus spp.*: advances and perspectives. Journal of Future Foods 1(2): 128–140. https://doi.org/10.1016/j.jfutfo.2022.01.002

Zhang, P., He, S., Wu, S., et al., 2022. Discovering a multi-component combination against vascular dementia from *danshen-honghua* herbal pair by spectrum-effect relationship analysis. Pharmaceuticals (Basel) 15(9): 1073. https://www.mdpi.com/1424-8247/15/9/1073

Zhang., G.P., Wang, Y.N., Qin, C.Q., et al., 2023. Structural characterization of an antioxidant polysaccharide isolated from the fruiting bodies of *Lyophyllum decastes*. Journal of Molecular Structure 1285: 8. https://doi10.1016/j.molstruc.2023.135507

Zhang, T.T., Hu, W., Chen, W. , *et al.*, 2021. Plasma membrane integrates biophysical and biochemical regulation to trigger immune receptor functions. Frontiers in Immunology 12: 8. https://doi.org/10.3389/fimmu.2021.613185

Zhou, Y., Chu, M.H., Ahmadi, F., et al., 2023. A comprehensive review on phytochemical profiling in mushrooms: occurrence, biological activities, applications and future prospective. Food Reviews International 40(3): 924–951. https://doi.org/10.1080/87559129.2023.2202738

Zhu, B.J., Nai, G.Y., Pan, T.X., et al., 2023. Combining network pharmacology and bioinformatics to identify bioactive compounds and potential mechanisms of action of *Sedum aizoon L* in the treatment of atherosclerosis. Quality Assurance and Safety of Crops & Foods 15(3): 104–116. https://doi.org/10.15586/qas.v15i3.1333

Zou, H., Zhou, C., Li, Y., et al., 2020. Speciation analysis of arsenic in edible mushrooms by high-performance liquid chromatography hyphenated to inductively coupled plasma mass spectrometry. Food Chemistry 327: 127033. https://doi10.1016/j.foodchem.2020.127033

Supplementary

Table S1. Detailed information on components identification of *L. edodes.*

No.	Components	Formula	Adducts	Precursor ions (m/z)	Peak area	Retention time (min)
1.	Oxidized fatty acids	$C_{18}H_{34}O_4$	[M-H]-	313.2379	389364	13.24663
2.	Organic acids	$C_6H_8O_7$	[M-H]-	191.0194	354182.7	1.903083
3.	Linoleic acids and derivatives	$C_{18}H_{30}O_4$	[M-H]-	309.2069	246438	12.98182
4.	Secondary alcohols	$C_9H_{17}NO_5$	[M-H]-	218.1031	197291.8	4.29345
5.	Oxidized fatty acids	$C_{18}H_{30}O_4$	[M-H]-	309.2074	79351.45	12.35152
6.	6-Alkyl amino purines	$C_{10}H_{13}N_5$	[M-H]-	202.1093	45440.13	2.145233
7.	3'-O-methylated flavonoids	$C_{16}H_{14}O_6$	[M-H]-	300.9998	39894.22	7.134133
8.	Diterpene glycosides	$C_{52}H_{82}O_{21}$	[M-H]-	1041.528	29063.5	8.181566
9.	Medium-chain fatty acids	$C_9H_{16}O_4$	[M-H]-	187.097	27965.81	8.1414
10.	Diarylethers	$C_{37}H_{41}ClN_2O_6$	[M-H]-	643.0568	22684.85	1.661933
11.	Phenylalanine and derivatives	$C_{12}H_{15}NO_4$	[M-H]-	236.0926	14982.2	7.6181
12.	Medium-chain hydroxy acids and derivatives	$C_6H_{12}O_7$	[M-H]-	195.0514	259383.6	1.541767
13.	Nucleoside and nucleotide analogues	$C_9H_{12}N_2O_6$	[M-H]-	243.0627	222588.6	1.862583
14.	Rotenones	$C_{23}H_{22}O_6$	[M-H]-	393.134	59459.38	5.595883
15.	Purine nucleosides	$C_{11}H_{14}N_4O_5$	[M-H]-	281.0896	45041.5	3.083017
16.	Sugar alcohols	$C_5H_{12}O_5$	[M-H]-	151.0615	27360.21	1.261617
17.	O-glucuronides	$C_8H_{14}O_7$	[M-H]-	221.0935	22846.38	5.028917
18.	Oligosaccharides	$C_{18}H_{32}O_{16}$	[M+H]+	543.1328	37676.8	1.29325
19.	Dipeptides	$C_{11}H_{20}N_2O_5$	[M-H]-	259.1294	36801.76	6.284517
20.	Gallic acid and derivatives	$C_{14}H_{21}N_3O_5$	[M+H]+	334.1407	32429.91	9.160983
21.	Fatty acyl glycosides of mono- and disaccharides	$C_{11}H_{17}NO_6$	[M-H]-	258.0976	20816.99	6.406
22.	Dicarboxylic acid and derivatives	$C_{20}H_{34}O_7$	[M+H]+	409.2202	15026.07	10.57958
23.	Beta hydroxy acid (BHAs) and derivatives	$C_5H_8O_5$	[M-H]-	147.0291	66964.04	1.903083
24.	Tricarboxylic acids and derivatives	$C_6H_6O_6$	[M+H]+	192.0512	42917.2	4.683067
25.	Purine nucleosides	$C_{10}H_{13}N_5O_4$	[M-H]-	266.0905	35266.7	2.145233
26.	Long-chain fatty acids	$C_{16}H_{32}O_3$	[M-H]-	271.227	20259.31	18.42863
27.	Peptides	$C_{11}H_{18}N_2O_4$	[M-H]-	241.1199	18800.83	6.60765
28.	Nicotinamides	$C_{13}H_{12}N_2O_2$	[M-H]-	227.0798	15118.66	1.261617
29.	N-acetylneuraminic acid	$C_{11}H_{19}NO_9$	[M-H]-	308.0997	45247.01	1.261617
30.	Flavonoid O-glycosides	$C_{21}H_{20}O_{11}$	[M-H]-	447.2018	23633.68	12.31135
31.	Long-chain fatty acids	$C_{18}H_{34}O_5$	[M-H]-	329.2351	198892.7	11.36573
32.	N-fructosyl amino acids	$C_{11}H_{17}NO_8$	[M-H]-	290.0861	31198.29	1.862583
33.	Cinnamic acid and derivatives	$C_9H_{10}O_3$	[M-H]-	165.0568	25600.38	7.457117
34.	O-glycosyl compounds	$C_{22}H_{36}O_{12}$	[M-H]-	491.2145	23579.73	7.0938
35.	Naphthopyranones	$C_{28}H_{22}O_{10}$	[M+H]+	557.149	59677.49	1.372917
36.	Phenolic glycosides	$C_{18}H_{18}O_9$	[M-H]-	377.0864	50035.88	1.261617
37.	Prenylated isoflavones	$C_{21}H_{20}O_5$	[M-H]-	351.1205	22181.2	6.001017
38.	Indoline	C_8H_9N	[M+H]+	120.0822	54571.89	3.703167
39.	Amino acids	$C_{10}H_{15}NO_4$	[M-H]-	212.0914	14093.35	8.543384
40.	3-O-methylated flavonoids	$C_{16}H_{12}O_7$	[M+H]+	334.0868	18400.59	1.5729
41.	Caffeic acid and derivatives	$C_{15}H_{18}O_9$	[M-H]-	341.0855	125466.6	4.4657

(*continues*)

Table S1. Continued.

No.	Components	Formula	Adducts	Precursor ions (m/z)	Peak area	Retention time (min)
42.	Terpene glycosides	$C_{23}H_{34}O_{16}$	[M-H]-	565.1792	36561.27	1.983583
43.	Xanthines	$C_6H_6N_4O_2$	[M-H]-	165.0401	30156.22	1.221283
44.	Dicarboxylic acids and derivatives	$C_4H_6O_4$	[M+H]+	119.0356	32159.07	4.683067
45.	Dipeptides	$C_8H_{16}N_2O_3$	[M-H]-	187.1105	57869.88	3.8903
46.	N-fructosyl amino acids	$C_{12}H_{23}NO_7$	[M-H]-	292.141	154678.1	2.1049
47.	O-glycosyl compounds	$C_{12}H_{22}O_{11}$	[M-H]-	341.1109	94117.92	1.261617
48.	Purine nucleosides	$C_{12}H_{17}N_5O_5$	[M-H]-	310.1134	40945.61	1.421617
49.	Flavonoid-7-O-glycosides	$C_{20}H_{22}O_{10}$	[M-H]-	421.1041	21765.38	1.261617
50.	Perfluorosulfonic acid (PFSA)	$C_3HClF_6O_4S$	[M-H]-	280.9092	35606.07	4.745433
51.	21-Hydroxysteroids	$C_{21}H_{30}O_5$	[M-H]-	361.1995	22452.5	15.78948
52.	Indole-3-acetic acid and derivatives	$C_{10}H_9NO_2$	[M-H]-	174.0589	23899.34	8.743867
53.	Phenolic glycosides	$C_{24}H_{34}O_9$	[M-H]-	465.21	19084.85	10.28078
54.	Phenylquinolines	$C_{23}H_{24}N_2O$	[M-H]-	343.1847	30786.72	8.10125
55.	Glutamic acid and derivatives	$C_{21}H_{22}N_4O_6S$	[M-H]-	457.1156	33433.43	1.4616
56.	Phenolic glycosides	$C_{16}H_{24}O_7$	[M-H]-	327.1415	27273.35	1.221283
57.	Pyrimidine nucleosides	$C_9H_{13}N_3O_5$	[M-H]-	242.0817	16997.86	10.44595
58.	7-O-methylisoflavones	$C_{21}H_{22}O_8$	[M-H]-	401.2393	43095.44	14.29997
59.	Saccharolipids	$C_{32}H_{56}O_{14}$	[M+H]+	687.3612	33179.88	7.409417
60.	Coumarin and derivatives	$C_{12}H_{10}O_4$	[M-H]-	217.0469	28455.31	1.221283
61.	Phenolic glycosides	$C_{14}H_{17}NO_8$	[M-H]-	326.1235	549333.8	3.566817
62.	Germacranolides and derivatives	$C_{22}H_{30}O_8$	[M-H]-	421.183	63248.78	5.474383
63.	Saccharolipids	$C_{21}H_{34}O_{10}$	[M+H]+	447.2263	39286.58	9.160983
64.	Dipeptides	$C_9H_{18}N_2O_3$	[M-H]-	201.123	51130.34	3.849817
65.	7-O-methylated flavonoids	$C_{19}H_{18}O_7$	[M-H]-	357.1019	29381.62	1.181117
66.	Hydroxypyrimidines	$C_5H_7N_3O_2$	[M+H]+	142.065	22333.67	5.2352
67.	Phenolic glycosides	$C_{13}H_{18}O_8$	[M+H]+	341.0672	12574.11	10.38377
68.	Medium-chain fatty acids	$C_{10}H_{18}O_4$	[M-H]-	201.1131	62232.11	8.9907
69.	Indoline	$C_{16}H_{10}N_2O_2$	[M-H]-	261.0627	17371.99	1.261617
70.	Macrolides and analogues	$C_{16}H_{20}O_6$	[M-H]-	307.1142	36616.81	1.221283
71.	Chromeno[2,3-b]pyridine-5-ones	$C_{16}H_{14}N_2O_4$	[M-H]-	297.0834	48058.59	1.5016
72.	Hydroxy fatty acids	$C_7H_{12}O_5$	[M-H]-	175.0606	45316.15	5.839366
73.	Glutamic acid and derivatives	$C_5H_9NO_4$	[M-H]-	146.0458	95387.94	1.221283
74.	Purine nucleosides	$C_{10}H_{13}N_5O_5$	[M-H]-	282.085	436324.4	2.024083
75.	Oxolanes	$C_{11}H_{20}O_4$	[M-H]-	215.0833	83713.98	6.001017
76.	Leucine and derivatives	$C_6H_{13}NO_2$	[M-H]-	130.0871	79256.39	2.064567
77.	Sugar alcohols	$C_6H_{14}O_6$	[M-H]-	181.0717	592400.9	1.261617
78.	Indole	C_9H_9N	[M+H]+	132.0803	42559.17	3.743117
79.	Naphthofurans	$C_{33}H_{42}N_2O_6$	[M+H]+	1125.622	99433.64	6.97645
80.	Alpha amino acids and derivatives	$C_5H_7NO_3$	[M-H]-	128.0369	137024.4	1.421617
81.	Flavonoid-7-O-glycosides	$C_{33}H_{40}O_{15}$	[M-H]-	675.237	42808.21	3.566817
82.	Steviol glycosides	$C_{32}H_{50}O_{13}$	[M+H]+	643.3314	30073.94	7.205767
83.	Linoleic acid and derivatives	$C_{18}H_{32}O_2$	[M-H]-	279.2319	95280.72	19.10748
84.	Oxidized fatty acids	$C_{18}H_{34}O_5$	[M-H]-	329.2325	648702.8	10.28078
85.	Linoleic acid and derivatives	$C_{18}H_{30}O_2$	[M-H]-	277.216	11723.33	18.10755

(*continues*)

Table S1. Continued.

No.	Components	Formula	Adducts	Precursor ions (m/z)	Peak area	Retention time (min)
86.	3-Alkylindoles	C_9H_9NO	[M+H-H_2O]+	130.0662	40869.95	3.703167
87.	Oxidized fatty acids	$C_{18}H_{32}O_4$	[M-H]-	311.2222	774960.1	12.31135
88.	Alkaloids	$C_{23}H_{30}N_2O_4$	[M-H]-	397.219	72047.72	10.28078
89.	Coumarins and derivatives	$C_{15}H_{16}O_4$	[M-H]-	259.0548	17378.57	10.36578
90.	Purine nucleosides	$C_{10}H_{12}N_4O_5$	[M-H]-	267.073	87090.22	2.024083
91.	Pyrenes	$C_{16}H_{10}O$	[M-H]-	217.0721	73213.62	5.474383
92.	Amino acids	$C_9H_{11}NO_2$	[M-H]-	164.0713	297771.6	3.405
93.	Steroidal saponins	$C_{38}H_{60}O_{12}$	[M+Na]+	731.3843	30056.7	7.57175
94.	Purine nucleosides	$C_{10}H_{12}N_4O_6$	[M-H]-	283.0699	97514.69	2.508383
95.	Alpha amino acids and derivatives	$C_4H_6N_2O_2$	[M+H]+	115.055	150391.1	5.2352
96.	BHAs and derivatives	$C_4H_6O_5$	[M+H]+	135.0319	97262.93	2.057717
97.	Alpha amino acids and derivatives	$C_3H_6N_2O_2$	[M+H]+	103.0556	131141.7	3.4952
98.	Quinolones and derivatives	$C_9H_7NO_2$	[M+H]+	162.0558	50670.63	1.733733
99.	Cardenolide glycosides and derivatives	$C_{41}H_{64}O_{14}$	[M+H]+	803.4265	21263.3	7.9019
100.	Organic acids	$C_4H_6O_4$	[M-H]-	117.0195	24347.64	1.5016
101.	Medium-chain hydroxy acids and derivatives	$C_{10}H_{20}O_3$	[M-H]-	187.132	53034.64	9.269183
102.	Delta valerolactones	$C_{24}H_{36}O_5$	[M+H]+	427.2336	37145.64	7.942234
103.	Medium-chain hydroxy acids and derivatives	$C_6H_{12}O_7$	[M-H]-	195.0509	332932.5	1.221283
104.	Indole and derivatives	$C_{10}H_{11}NO$	[M+H]+	144.0814	41152.14	6.0575
105.	Tricarboxylic acids and derivatives	$C_6H_8O_7$	[M-H]-	191.0196	183291.3	1.381283
106.	Coumaric acid and derivatives	$C_{31}H_{38}O_{17}$	[M+H]+	705.1863	24483.38	1.29325
107.	Cardenolide glycosides and derivatives	$C_{49}H_{76}O_{19}$	[M+H]+	991.5059	29161.29	8.063884
108.	Purine nucleosides	$C_{11}H_{15}N_5O_5$	[M-H]-	296.0985	75328.03	2.957017
109.	Indolyl carboxylic acids and derivatives	$C_{11}H_{12}N_2O_2$	[M-H]-	203.0825	189869.1	5.191233
110.	6,7-dihydroxycoumarins	$C_{10}H_8O_4$	[M+H]+	193.0501	13898.28	10.38377
111.	L-alpha-amino acids	$C_5H_9NO_4$	[M+H]+	148.0625	87936.63	1.693733
112.	BHAs and derivatives	$C_4H_6O_5$	[M-H]-	133.0139	270234.9	1.381283
113.	7-O-methylated isoflavonoids	$C_{22}H_{26}O_5$	[M+H]+	393.1607	28570.62	1.5729
114.	Vitamin K compounds	$C_{15}H_{14}O_3$	[M-H]-	241.0834	73192.02	3.364833
115.	Precocenes	$C_{15}H_{18}O_4$	[M+H]+	263.1386	34388.84	9.160983
116.	Alkaloids and derivatives	$C_{11}H_{16}N_2O_2$	[M+H]+	209.1306	15719.67	12.60347
117.	Sulfinic acid	$C_2H_7NO_2S$	[M+H]+	110.0356	34988.04	2.057717
118.	Aryl alkyl ketones	$C_{30}H_{40}NNaO_4$	[M+H]+	502.2927	92229.73	12.60347
119.	Hydroxypyrimidines	$C_5H_6N_2O_2$	[M+H]+	127.0566	18418.14	6.0575
120.	Carbazoles	$C_{12}H_{11}NO$	[M+H]+	208.0848	26025.08	1.693733

Table S2. Detailed information on the components identification of *L. decastes*.

No.	Components	Formula	Adducts	Precursor ions (m/z)	Peak area	Retention time (min)
1.	Oxidized fatty acids	$C_{18}H_{34}O_5$	[M-H]-	329.2328	688134.6	11.24757
2.	Oxidized fatty acids	$C_{18}H_{30}O_4$	[M-H]-	309.206	549905.2	12.16518
3.	Secondary alcohols	$C_9H_{17}NO_5$	[M-H]-	218.1035	332371.8	1.882917
4.	Oxidized fatty acids	$C_{18}H_{32}O_6$	[M-H]-	343.2122	249427.7	10.88658
5.	Isobenzofurans	$C_{12}H_{20}O_6$	[M-H]-	259.1188	99500.4	7.545767
6.	Tricarboxylic acids and derivatives	$C_6H_8O_7$	[M-H]-	191.0197	87099.98	1.320283
7.	Hydrolyzable tannins	$C_{14}H_6O_8$	[M-H]-	300.9989	74182.92	7.099133
8.	Lipids	$C_{23}H_{44}NO_7P$	[M-H]-	476.2775	67559.25	14.3249
9.	Dipeptides	$C_{11}H_{20}N_2O_5$	[M-H]-	259.1297	62994.46	1.400433
10.	Long-chain fatty acids	$C_{16}H_{32}O_3$	[M-H]-	271.2279	59068.56	18.39802
11.	Phenoxyacetic acid derivatives	$C_{20}H_{32}O_4$	[M+H]+	359.2187	48512.67	13.0559
12.	Alkyl-phenylketones	$C_{18}H_{28}ClNO_2$	[M+H]+	290.2108	40847.5	8.422833
13.	Isoindolones	$C_{25}H_{35}NO_5$	[M+H]+	447.2852	34771.75	16.38438
14.	Gluco/mineralocorticoids, progestogins and derivatives	$C_{27}H_{30}Cl_2O_6$	[M+H]+	543.1307	33428.57	1.163717
15.	Medium-chain fatty acids	$C_9H_{16}O_4$	[M-H]-	187.0977	30968.6	8.744534
16.	Leucothol and grayanotoxane diterpenoids	$C_{22}H_{36}O_7$	[M+H]+	430.2798	27825.4	8.995133
17.	Medium-chain fatty acids	$C_{12}H_{22}O_6$	[M-H]-	261.1345	24333.88	7.058633
18.	N-fructosyl amino acids	$C_{12}H_{23}NO_7$	[M-H]-	292.1393	21977.02	1.681083
19.	Dipeptides	$C_{14}H_{18}N_2O_3$	[M-H]-	261.1248	478412.1	5.6777
20.	Prenylated flavanones	$C_{25}H_{28}O_4$	[M-H]-	391.1892	250268	10.5256
21.	Long-chain fatty acids	$C_{18}H_{34}O_3$	[M-H]-	297.2432	37254.85	17.10558
22.	Medium-chain fatty acids	$C_{12}H_{20}O_4$	[M-H]-	227.1294	27128.78	8.785033
23.	3-Methylindoles	C_9H_9N	[M-H]-	130.0666	21324.65	8.42155
24.	Indole-3-acetic acid derivatives	$C_{10}H_9NO_2$	[M-H]-	174.0557	19317.33	8.42155
25.	Quassinoids	$C_{20}H_{30}O_8$	[M-H]-	397.1863	11529.69	8.110733
26.	Nucleoside and nucleotide analogues	$C_9H_{12}N_2O_6$	[M-H]-	243.0629	189407.9	1.400433
27.	Oxidized fatty acids	$C_{18}H_{34}O_3$	[M-H]-	297.2429	153862.4	17.38823
28.	Dipeptides	$C_{13}H_{16}N_2O_5$	[M-H]-	279.098	78626.05	2.861033
29.	Methoxyphenols	$C_{11}H_{14}O_4$	[M-H]-	209.0812	71460.02	8.110733
30.	Alkyl-phenylketones	$C_{15}H_{17}NO_4$	[M-H]-	274.1189	69269.67	5.191067
31.	Medium-chain fatty acids	$C_{15}H_{23}NO_4$	[M-H]-	280.156	32681.96	10.5256
32.	Medium-chain fatty acids	$C_{10}H_{18}O_4$	[M-H]-	201.1139	27231.96	8.987017
33.	O-glycosyl compounds	$C_{12}H_{22}O_{11}$	[M-H]-	341.1097	190576.7	2.124567
34.	Medium-chain fatty acids	$C_7H_{12}O_4$	[M-H]-	159.0655	53388.01	5.7182
35.	Cholines	$C_5H_{14}NO$	[M+H]+	104.1078	45776.67	8.543317
36.	Oxolanes	$C_{11}H_{20}O_4$	[M-H]-	215.1297	26657.86	9.834483
37.	Phenolic glycosides	$C_{12}H_{16}O_6$	[M-H]-	255.0882	26324.81	6.124183
38.	Glutamic acid and derivatives	$C_{21}H_{22}N_4O_6S$	[M-H]-	457.1197	291020.1	1.360433
39.	Flavonoid 8-C-glycosides	$C_{26}H_{28}O_{14}$	[M-H]-	563.2087	124534.1	2.251083
40.	Sesquiterpenoids	$C_{30}H_{30}O_8$	[M-H]-	517.1877	38981.13	1.200617
41.	N-acyl-alpha amino acids	$C_8H_{16}N_2O_3$	[M-H]-	187.1071	38002.27	1.400433
42.	Pyridines and derivatives	$C_{12}H_{17}N_5$	[M-H]-	230.142	26419.77	6.57165
43.	Triterpenoids	$C_{30}H_{40}O_4$	[M+H]+	465.296	19141.55	15.35178

(*continues*)

Table S2. Continued.

No.	Components	Formula	Adducts	Precursor ions (m/z)	Peak area	Retention time (min)
44.	Purine nucleosides	$C_{10}H_{13}N_5O_5$	[M-H]-	282.0854	131522.8	1.6411
45.	Flavonoid O-glycosides	$C_{21}H_{20}O_{11}$	[M-H]-	447.1997	37202.37	13.47867
46.	Butenolides	$C_9H_{14}O_4$	[M-H]-	185.083	22890.21	9.552167
47.	Naphthopyrans	$C_{21}H_{28}O_6$	[M-H]-	375.1825	140189.2	12.87817
48.	21-Hydroxysteroids	$C_{21}H_{30}O_5$	[M-H]-	361.2008	135548.9	15.36285
49.	Flavonoid O-glycosides	$C_{21}H_{22}O_{10}$	[M-H]-	433.1739	35099.22	6.936967
50.	Imidazolyl carboxylic acid and derivatives	$C_{10}H_{18}N_2O_3$	[M-H]-	213.1228	28937.12	1.72125
51.	1,4-Dioxanes	$C_{14}H_{24}N_2O_7$	[M-H]-	331.1523	27146.39	6.205184
52.	Oligopeptides	$C_{19}H_{27}N_3O_6$	[M-H]-	392.1841	89753.66	7.058633
53.	Medium-chain hydroxy acids and derivatives	$C_{11}H_{18}O_5$	[M-H]-	229.1068	70034.16	8.58305
54.	Naphthalenes	$C_{21}H_{25}N$	[M+H]+	292.2046	19484.05	12.57427
55.	Indoles and derivatives	$C_{16}H_{23}N_5O$	[M-H]-	300.1814	25168.98	9.310184
56.	Fatty acid esters	$C_{21}H_{36}O_6$	[M-H]-	383.2422	100392.2	14.08692
57.	Peptides	$C_{12}H_{24}N_2O_3$	[M-H]-	243.1733	45353.91	5.63705
58.	Acyloins	$C_{21}H_{30}O_5$	[M-H]-	361.2041	118311.8	15.36285
59.	Oligopeptides	$C_{28}H_{44}N_4O_4$	[M-H]-	499.3311	22417.2	12.38345
60.	O-glucuronides	$C_8H_{14}O_7$	[M-H]-	221.0919	290090.6	2.660033
61.	Isoflavones	$C_{15}H_{10}O_5$	[M-H]-	269.0551	60320.98	8.542883
62.	Oxime ethers	$C_7H_{10}N_4O_3$	[M-H]-	235.1112	58757.01	2.619717
63.	Furopyrans	$C_{26}H_{32}O_8$	[M+H]+	473.2118	22371.86	5.646584
64.	Phenolic glycosides	$C_{18}H_{18}O_9$	[M-H]-	377.0854	268756.6	1.200617
65.	Medium-chain fatty acids	$C_{14}H_{18}O_5$	[M-H]-	265.1057	46270.35	8.030416
66.	3',5'-Cyclic purine nucleotides	$C_{10}H_{12}N_5O_6P$	[M-H]-	328.0477	17821.92	1.6411
67.	3-Alkylindoles	$C_{13}H_{16}N_2O_2$	[M-H]-	231.1245	32742.01	7.7481
68.	Phenolic glycosides	$C_{14}H_{17}NO_8$	[M-H]-	326.1246	37233.94	1.76175
69.	Dicarboxylic acid and derivatives	$C_4H_6O_4$	[M+H]+	119.0369	153099.9	1.602367
70.	Cinnamic acid and derivatives	$C_{18}H_{21}NO_4$	[M-H]-	314.1139	45394.23	7.058633
71.	Limonoids	$C_{26}H_{36}O_7$	[M+H]+	483.3055	30284.66	12.06363
72.	Eudesmanolides, secoeudesmanolides, and derivatives	$C_{25}H_{38}O_{12}$	[M-H]-	529.2255	58202.28	1.84275
73.	Phosphatidylcholines	$C_{42}H_{82}NO_8P$	[M+H]+	760.5799	178083.9	15.63423
74.	Short-chain keto acids and derivatives	$C_5H_8O_3$	[M+H]+	117.0581	46462.05	1.88935
75.	Indolyl carboxylic acids and derivatives	$C_{11}H_{12}N_2O_2$	[M-H]-	203.0828	528820.9	3.034817
76.	Benzoic acid esters	$C_{14}H_{15}N_5O_6S$	[M-H]-	380.0634	29223.68	1.6011
77.	Steroid esters	$C_{31}H_{48}O_6$	[M-H]-	515.3584	21294.85	14.20557
78.	Naphthopyrans	$C_{28}H_{36}O_7$	[M-H]-	483.2335	47921.86	9.390667
79.	Alkyl-phenylketones	$C_{22}H_{22}FN_3O_2$	[M-H]-	378.1661	112742.9	6.408834
80.	Phenolic glycosides	$C_{15}H_{18}O_8$	[M-H]-	325.1616	83333.98	14.24523
81.	Isoindolones	$C_{24}H_{35}NO_4$	[M-H]-	400.2318	43089.91	14.08692
82.	C20-Gibberellin 6-carboxylic acids	$C_{20}H_{26}O_5$	[M-H]-	345.1666	27058.02	7.343117
83.	Phenylalanine and derivatives	$C_9H_{11}NO_2$	[M-H]-	164.0717	294260.7	1.80225
84.	Hydroxy fatty acids	$C_7H_{12}O_5$	[M-H]-	175.0614	245560.1	4.853917
85.	Flavonoid-7-O-glycosides	$C_{27}H_{30}O_{15}$	[M-H]-	593.2231	74361.05	2.003733
86.	Glutamine and derivatives	$C_{28}H_{38}N_2O_7$	[M+H]+	515.2795	39850.05	9.115617

(*continues*)

Table S2. Continued.

No.	Components	Formula	Adducts	Precursor ions (m/z)	Peak area	Retention time (min)
87.	Naphthopyranones	$C_{14}H_8O_6$	[M-H]-	271.0136	39124.95	10.23745
88.	Lipids	$C_{27}H_{54}NO_{12}P$	[M-H]-	614.3338	71140.57	8.542883
89.	Lipids	$C_{26}H_{50}NO_7P$	[M+H]+	520.3397	42430.07	14.5195
90.	Oxidized fatty acids	$C_{18}H_{32}O_4$	[M-H]-	311.2226	2047702	13.38845
91.	Alpha amino acids and derivatives	$C_3H_7N_3O_2$	[M-H]-	116.0515	48463.46	6.85615
92.	BHAs and derivatives	$C_4H_6O_5$	[M+H]+	135.0305	49891.13	1.683867
93.	7-O-Methylated flavonoids	$C_{19}H_{18}O_7$	[M-H]-	357.1031	19128.16	1.160783
94.	Biphenyls and derivatives	$C_{18}H_{22}O_6$	[M-H]-	333.1292	47906.8	5.47505
95.	2'-Hydroxy-dihydrochalcones	$C_{15}H_{14}O_4$	[M-H]-	257.1035	56146.97	8.030416
96.	Long-chain fatty acids	$C_{16}H_{32}O_2$	[M-H]-	255.2331	19809.23	20.24078
97.	Hydroquinolones	C_9H_7NO	[M-H]-	144.0465	68995.61	8.116533
98.	Leucine and derivatives	$C_6H_{13}NO_2$	[M-H]-	130.0873	155203.4	1.6411
99.	Naphthofurans	$C_{20}H_{28}O_3$	[M+Na]+	339.1891	14199.97	15.7706
100.	3-Alkylindoles	C_9H_9NO	[M+H-H2O]+	130.0659	29115.12	8.422833
101.	Linoleic acid and derivatives	$C_{18}H_{32}O_2$	[M-H]-	279.2327	149488	19.10913
102.	Long-chain fatty acids	$C_{18}H_{34}O_2$	[M-H]-	281.2493	47593.36	20.36357
103.	Ketals	$C_{36}H_{61}NaO_{11}$	[M+H]+	694.389	39496.04	1.724517
104.	1,4-Benzodiazepines	$C_{17}H_{14}N_2O_2$	[M-H]-	277.1546	24834.18	6.61215
105.	Hydroxybenzaldehydes	$C_{23}H_{29}ClO_4$	[M-H]-	403.2713	22729.26	9.914967
106.	Oxidized fatty acids	$C_{18}H_{34}O_4$	[M-H]-	313.2387	239890.3	12.70548
107.	Stilbenes	$C_{14}H_{12}O_3$	[M-H]-	227.1403	164394.3	1.92325
108.	Indoles	C_9H_9N	[M+H]+	132.082	41733.77	6.142617
109.	Chromones	$C_{13}H_{14}O_4$	[M-H]-	233.0757	17061.21	1.160783
110.	Naphthofurans	$C_{20}H_{34}O_4$	[M+Na]+	361.2313	24442.77	14.09052
111.	Cinnamaldehydes	$C_9H_8O_2$	[M-H]-	147.0448	21781.39	1.80225
112.	Alkaloids	$C_{23}H_{30}N_2O_4$	[M-H]-	397.2198	173761.3	10.35678
113.	Linear diarylheptanoids	$C_{19}H_{20}O_5$	[M-H]-	327.1941	14524.31	7.5861
114.	N-acyl amines	$C_{20}H_{36}N_4O_8$	[M+H]+	483.2491	54466.5	14.5195
115.	Histidine and derivatives	$C_9H_{15}N_3O_2S$	[M-H]-	228.0879	32241.37	6.287017
116.	Alpha amino acids and derivatives	$C_4H_6N_2O_2$	[M+H]+	115.0565	87360.12	6.142617
117.	Indoles and derivatives	$C_{24}H_{26}N_2O_2$	[M+H]+	375.2136	41256.94	10.32722
118.	Flavins	$C_{17}H_{20}N_4O_6$	[M-H]-	375.1325	46508.74	6.124183
119.	Phenylpiperidines	$C_{22}H_{28}N_2O_2$	[M+H]+	353.2285	21989.78	10.28705
120.	Oxidized fatty acids	$C_9H_{18}O_3$	[M-H]-	173.1177	15370.58	8.259733
121.	Cerveratrum-type alkaloids	$C_{27}H_{43}NO_3$	[M+H]+	452.3127	247793.1	8.875134
122.	Indoles	C_8H_7N	[M+H]+	118.0668	90743.75	2.753133
123.	Organic acids	$C_{10}H_{18}O_5$	[M-H]-	217.1077	66271.49	7.343117
124.	Cardenolide glycosides and derivatives	$C_{29}H_{44}O_9$	[M+H]+	559.2831	18728.07	6.142617
125.	Aconitane-type diterpenoid alkaloids	$C_{25}H_{41}NO_7$	[M+H]+	468.3044	41632.81	7.88835
126.	Phosphocholines	$C_5H_{15}NO_4P$	[M+H]+	184.0741	73973.06	6.547433
127.	Alpha amino acids and derivatives	$C_3H_6N_2O_2$	[M+H]+	103.0542	177650	1.88935
128.	Glutamic acid and derivatives	$C_5H_9NO_4$	[M-H]-	146.0446	32350.85	1.200617
129.	Alpha amino acids	$C_4H_7NO_2$	[M+H]+	102.0476	43224.8	1.88935
130.	Ketals	$C_{26}H$	[M+H]+	429.2699	39331.47	8.9153

(*continues*)

Table S2. Continued.

No.	Components	Formula	Adducts	Precursor ions (m/z)	Peak area	Retention time (min)
131.	Tyrosine and derivatives		[M+H]+	198.0653	29220.79	6.102283
132.	BHAs and derivatives	$_{36}O_5$	[M-H]-	133.0139	338616.7	1.320283
133.	Alkaloids and derivatives	$C_9H_{11}NO_4$	[M+H]+	209.1313	18565.44	12.57427
134.	Strychnos alkaloids	$C_4H_6O_5$	[M-H]-	353.1841	30656.95	14.8629
135.	Kaurane diterpenoids	$C_{11}H_{16}N_2O_2$	[M+H]+	376.2572	230025.8	12.57427
136.	Benzazepines	$C_{21}H_{26}N_2O_3$	[M+H]+	412.2065	19489.04	8.543317
137.	Sulfinic acid	$C_{22}H_{33}NO_4$	[M+H]+	110.0358	21117.81	1.683867
138.	Aconitane-type diterpenoid alkaloids	$C_{24}H_{29}NO_5$	[M+H]+	466.2893	61282.63	7.807367
139.	Pyridines and derivatives	$C_2H_7NO_2S$	[M+H]+	184.0741	129057.4	8.503317
140.	Fluorenes	$C_{25}H_{39}NO_7$	[M+H]+	432.2973	23864.71	11.78715
141.	Dicarboxylic acid and derivatives	$C_{10}H_{11}NO$	[M-H]-	115.0043	89568.43	1.320283
142.	Tricarboxylic acid and derivatives	$C_{27}H_{39}NO_2$	[M-H]-	191.0196	388035.5	1.681083
143.	Naphthopyrans	$C_4H_4O_4$	[M-H]-	441.2347	21192.03	6.246
144.	Indole-3-acetic acid derivatives	$C_6H_8O_7$	[M-H]-	174.0554	17986	7.38395

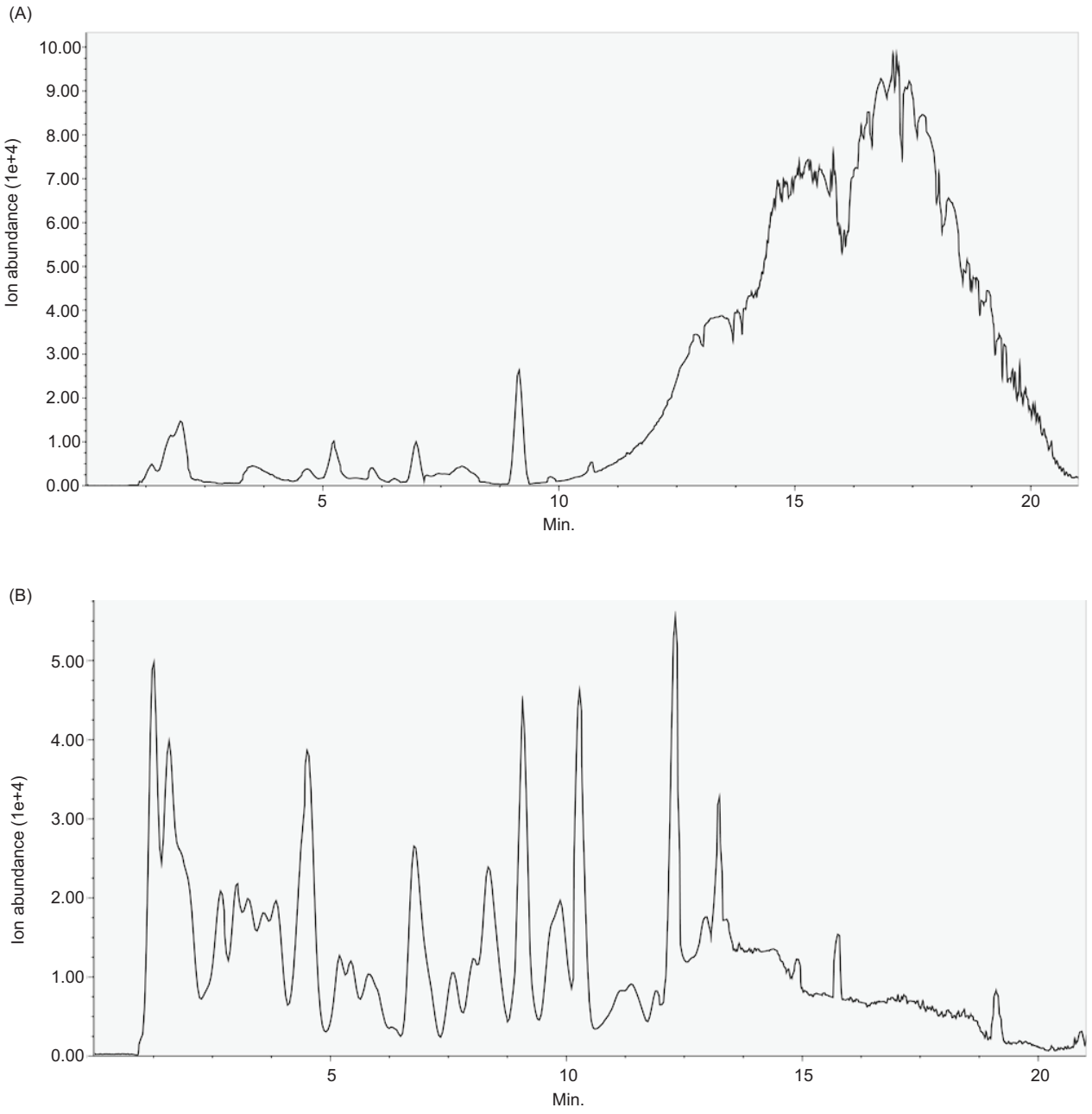

Figure S1. Full-scan ion abundance profile chromatogram in different ion modes of *L. edodes* and *L. decastes*. (A) Positive ion mode chromatogram of *L. edodes*, (B) negative ion mode chromatogram of *L. edodes*.

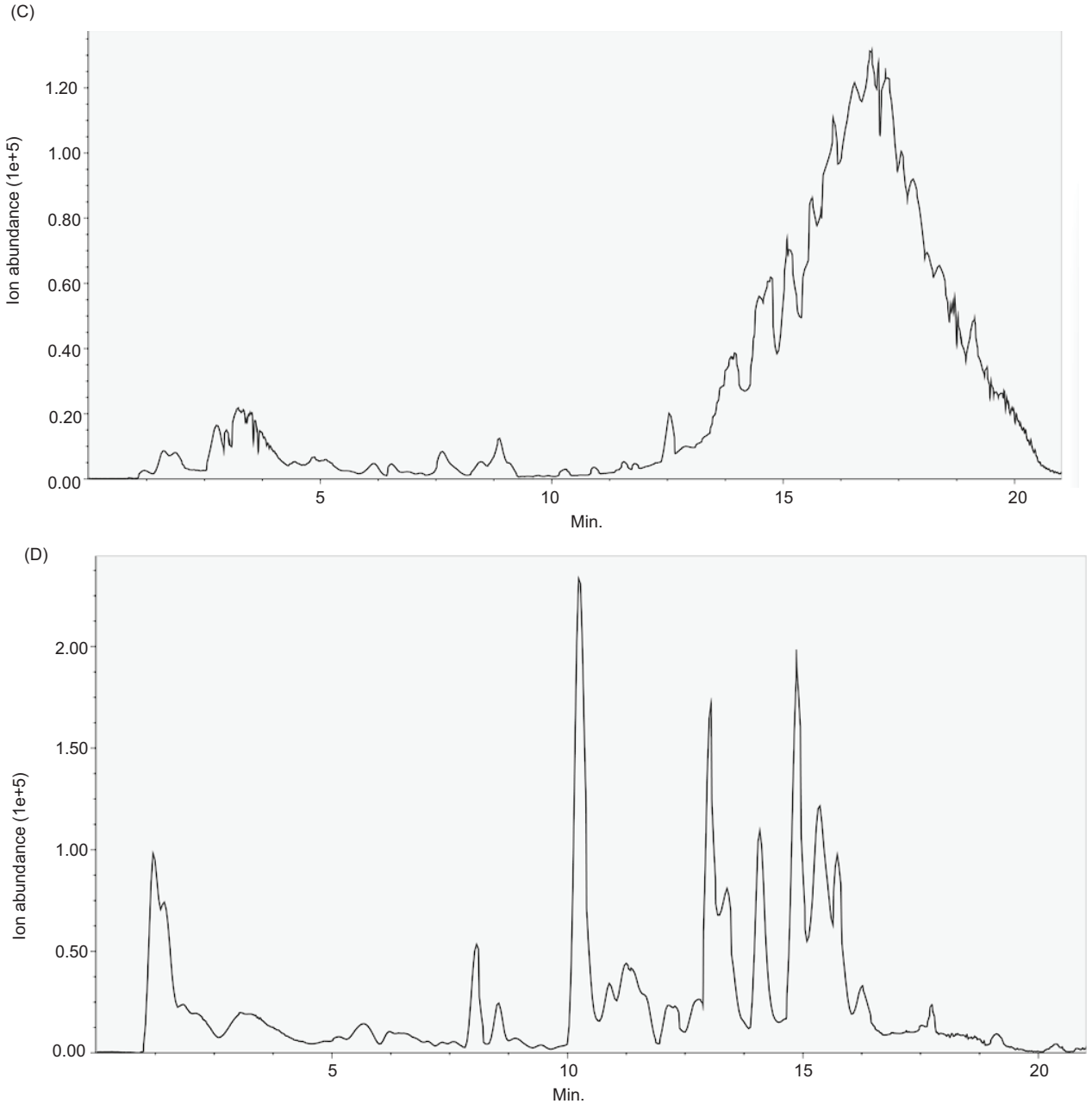

Figure S1. Full-scan ion abundance profile chromatogram in different ion modes of *L. edodes* and *L. decastes*. (C) positive ion mode chromatogram of *L. decastes*, and (D) negative ion pattern chromatogram of *L. decastes*.